PHYSICAL REVIEW LETTERS

VOLUME 7 AUGUST 1, 1961 NUMBER 3

SCREW INSTABILITY OF A PLASMA COLUMN

F. C. Hoh and B. Lehnert
Royal Institute of Technology, Stockholm, Sweden

(Received July 3, 1961)

In earlier experiments with the positive column an instability has been observed in the presence of a longitudinal magnetic field.[1-3] A theoretical explanation of the phenomenon has been given by Kadomtsev and Nedospasov[4] who discuss the growth of a screw-shaped disturbance in the plasma column. Recent experiments support the theory.[5,6] Even if the physical and mathematical assumptions of the theory seem to be well founded, the mechanism of the instability has not yet been fully explained. In particular, the role which the $\vec{i}\times\vec{B}$ force plays is not very clear. In this Letter an attempt will be made to interpret the results physically.

According to the theory[4] the plasma is stable for a screw disturbance of the form $\exp(ikz+im\psi-i\omega t)$ with $m=1$ if

$$KX^4+FX^2+G_d+G_\gamma \geq 0.163\frac{v_0}{\beta_0 D_e}X\frac{b_e}{b_i}, \qquad (1)$$

where

$$K=\frac{1.28+y}{y(y+1)};\quad F=\frac{0.8(y+2)}{y};$$
$$G_d=\frac{0.48(1+y)}{y};\quad G_\gamma=0.1\frac{b_e/b_i}{1+y}, \qquad (2)$$

and $X=k\Omega\tau/\beta_1$, $y=b_i(\Omega\tau)^2/b_e$, Ω is the gyrofrequency, τ the collision time, b_e the mobility, v_0 the axial velocity, and D_e the diffusion coefficient of electrons. Further, b_i is the mobility of ions and $\beta_0 a$ and $\beta_1 a$ are the first zeros of J_0 and J_1 with a indicating the tube radius. The collision frequency of ions is assumed to be much larger than their gyrofrequency.

Examination of relation (1) and the basic equations used in the theory[4] shows that the right-hand member contains the imposed electric field and represents the effects which destabilize the system. The stabilizing effects are provided by the left-hand member. In the first term, KX^4, are included dissipation effects due to diffusion and conduction of electrons along the magnetic field $\vec{B}_z$. The term G_d represents corresponding effects in the transverse direction for electrons and ions, and FX^2 contains a coupling of longitudinal and transverse dissipation effects. Finally, the term G_γ arises from a rotation, $\vec{E}_{0\gamma}\times\vec{B}_z/B_z^2$, of the perturbed electron distribution in the unperturbed ambipolar field $\vec{E}_{0\gamma}$ (see Fig. 1). Since ions are assumed to be unaffected by the magnetic field, they will lag behind the rotation of the electron distribution.

The sketch given in Fig. 1 shows a density perturbation of screw type superimposed on the unperturbed, steady-state distribution. With the directions given in the figure the axial electric field $\vec{E}_{0z}$ tends to "lift up" the electron screw relative to the ion screw. This is equivalent to a rotation of the electron screw in the positive ψ direction. Due to a subsequent charge separation an azimuthal electric field $\vec{E}_{\psi'}$ will arise which tends to drive the particles outwards with a speed $\vec{E}_{\psi'}\times\vec{B}_z/B_z^2$ and to destabilize the plasma. The pitch of the screw and its angular velocity $\vec{\omega}_\gamma$ as given in Fig. 1 are consistent with theory[4] and experiments.[5,6] The outward drift due to charge separation resembles that discussed earlier in connection with the stability of a plasma boundary.[7,8] In the latter case charge separation is pro-

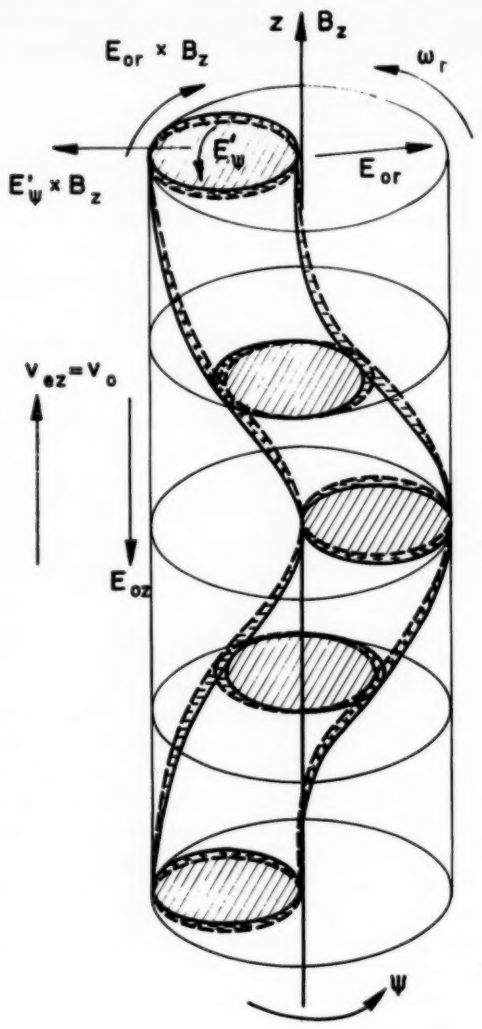

FIG. 1. Left-handed screw instability for $m = 1$. The perturbed density distribution of ions is given by the screw-shaped body confined by full lines. The corresponding electron distribution is indicated by dashed lines.

duced by drift motions across the magnetic field, whereas the separation in the present configuration arises from motions along the field.

On the other hand, the ambipolar electric field tends to rotate the electron screw in the negative ψ direction relative to the ion screw. The field $\vec{E}_{0r}$ has the direction shown in Fig. 1 under the prevailing experimental conditions, i.e., when no field reversal takes place near the critical magnetic field. This rotation counteracts the charge separation produced by the longitudinal electric field. In the special case where these two effects balance each other the electron screw will become steady, with electrons moving in screw-shaped paths inside the ion screw. It is then also seen that the balance takes place at a certain critical strength of the magnetic field. In reality the rotation will not be uniform as assumed in this simple description but the main features of the stability situation will still be the same.

Additional stabilizing effects are provided by diffusion and conduction which tend to smooth out the perturbed density and potential distributions and to suppress their asymmetry.

According to the present interpretation it is not unimaginable that the screw instability will exist in a large number of situations where there is a sufficiently large electric field component along the magnetic field. For the mechanism just described, the destabilizing action of this component does not depend upon the ionization degree and the instability can also be expected to arise in a fully ionized plasma.

[1]B. Lehnert, Proceedings of the Second United Nations International Conference on the Peaceful Uses of Atomic Energy, 1958 (United Nations, Geneva, 1958), Vol. 32, p. 349.

[2]F. C. Hoh and B. Lehnert, Phys. Fluids 3, 600 (1960).

[3]F. C. Hoh, Arkiv Fysik 18, 433 (1960).

[4]B. B. Kadomtsev and A. V. Nedospasov, J. Nuclear Energy, Part C, 1, 230 (1961).

[5]T. K. Allen, G. A. Paulikas, and R. V. Pyle, Phys. Rev. Letters 5, 409 (1960).

[6]G. A. Paulikas, University of California Radiation Laboratory Report UCRL-9588, 1961 (unpublished).

[7]M. N. Rosenbluth and C. L. Longmire, Ann. Phys. 1, 120 (1957).

[8]B. Lehnert, Phys. Fluids 4, 847 (1961); additional report to be published.

EXPERIMENTAL EVIDENCE FOR BEAM-PLASMA INTERACTION IN A LOW-PRESSURE ARGON DISCHARGE*

Lawrence H. Putnam,† Harry D. Collins,† and Norman L. Oleson
Department of Physics, U. S. Postgraduate School, Monterey, California
(Received June 30, 1961)

Akhiezer and Fainberg[1] and Bohm and Gross,[2] in theoretical investigations, have shown that the state of an unmodulated beam of electrons moving through a homogeneous plasma is unstable. Density and velocity fluctuations, arising in the beam or the plasma, may excite longitudinal plasma oscillations of growing amplitude in the plasma. Recent experimental results obtained in this laboratory tend to corroborate this theory.

Data have been taken in an argon discharge at 6.9 microns pressure. The discharge parameters were: current 50 ma, tube voltage 40 volts, cathode-anode separation 40 mm, cathode diameter 2 cm. A cylindrical Langmuir probe was used in the discharge at ten positions spaced 4 mm apart along the axial length of the tube. Probe potential was applied with respect to the anode by using a very slow (0.05 cps) triangle wave. Probe current, probe current squared, and first and second derivatives of probe current with respect to probe voltage were plotted vs applied probe potential automatically by means of an X-Y recorder. Derivatives were obtained electrically from simple RC differentiating circuits where the time constant was about 1/100 of the half-period of the driving triangle wave.

Second derivatives were then transformed into energy distribution functions by use of the expression[3]

$$N\phi(eV) = \frac{2}{Ae}\left(\frac{2m_e V_p}{e}\right)^{1/2} \frac{d^2 i_p}{dV_p^2},$$

where $N\phi(eV)$ is the number of electrons per unit of energy per unit volume, i.e., reciprocal electron volts and reciprocal cm^3, A is the area of the probe, m_e is the mass of the electron, e is the electronic charge, i_p is the probe current, and V_p is the probe voltage with respect to the anode.

Examination of the distribution functions for the ten probe positions between cathode and anode shows that two distinct groups of electrons are present out to 12 mm from the cathode, a low-energy group with an average energy of about 5 electron volts, and a higher energy group of about 22 electron volts average energy. At 16 mm from the cathode, the distribution function shows that the high-energy group of electrons (beam electrons) is starting to transfer energy to the low-energy group (random plasma electrons). All other distribution functions at distances greater than 16 mm from the cathode show only one group of electrons which is essentially Maxwellian in form. This fact indicates energy exchange is essentially complete. Three distribution functions, showing the gross changes, are illustrated in inserts (a), (b), and (c) to Fig. 1(A).

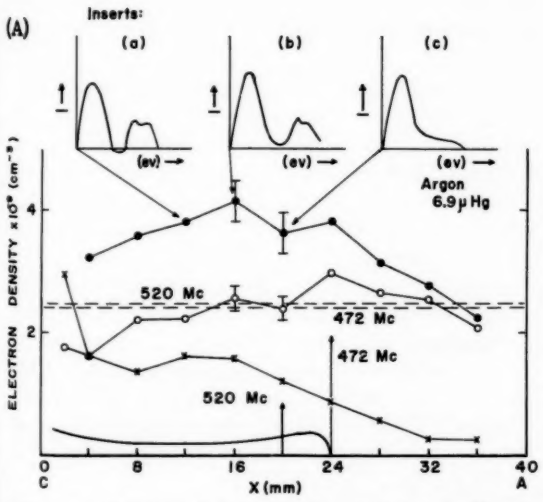

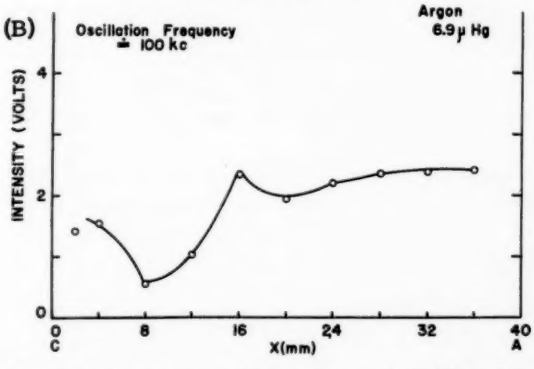

FIG. 1. Electron densities and associated oscillations as a function of cathode-probe distance. (A) Solid circles: total electron density (from distribution functions); open circles: plasma density (from distribution functions); crosses: intermediate energy beam electrons (from distribution function); solid curve: high-energy beam electrons (combined technique of J. F. Waymouth [Notes, Massachusetts Institute of Technology Summer School of Plasma Physics, 1958 (unpublished); J. Appl. Phys. 30, 1404 (1959)], and G. Medicus [J. Appl. Phys. 29, 903 (1958)]). (B) Ion oscillation intensity associated with curve -×- of Fig. 1(A).

Densities were computed by numerically integrating the energy distribution functions to obtain the random plasma electron density, beam electron density, and total electron density. In order to check the magnitudes of density obtained from the distribution functions, total electron density was also obtained from the slope of the probe current squared vs probe potential curves. Electron density as a function of cathode-probe distance is shown in Fig. 1(A).

Frequencies were measured with a cavity wavemeter inductively coupled to the probe at anode potential. Detected signals from the wavemeter crystal were fed into a dc micromicroammeter. A frequency of 520 Mc/sec was measured at a point 20 mm from the cathode. This frequency corresponded with the plasma density, rather than the total density, when the relation

$$\omega_0 = \frac{\omega_p}{(1 - S^2/v_0^2)^{1/2}},$$

cited by Kharchenko et al.,[1] was applied to it. Here ω_0 is the observed frequency in radians/sec, ω_p is the Langmuir plasma frequency, v_0 is the beam velocity, and S is the average thermal plasma velocity.

This frequency could only be detected in the vicinity of 20 mm from the cathode and could be associated with a decreasing plasma density gradient in accord with the contention by Allis[4] and the finding by Mahaffey et al.[5] that oscillations are initiated at or near a peak density gradient and grow in intensity down a decreasing density gradient. It is also significant to note that at this point (20 mm from the cathode) the beam density is starting to decrease, showing that breakup of the electron beam is occurring.

Another frequency of 472 Mc/sec was observed at 24 mm from the cathode. This observed frequency was also correlated with the plasma density and was associated with the decay of another higher energy beam of electrons (of an energy approximately equal to the tube voltage drop) which was present but does not show on the energy distribution functions because it was an order of magnitude smaller in density (see Fig. 1).

Ion oscillations of about 100 kc/sec were observed on the oscilloscope throughout the length of the tube. These oscillations were greatly disturbed in magnitude and wave shape in the interacting region, 16-20 mm from the cathode. A plot of ion oscillation intensity as a function of cathode-probe distance is shown in Fig. 1(B).

At a slightly lower pressure (5.9 microns) with discharge currents of 100 and 125 ma at a tube voltage of 20 volts with essentially the same cathode-anode separation (42 mm), high-energy electrons were detected. This phenomenon manifested itself in a disturbance to the probe characteristic curve at a point in the tube which was associated with either a peak density gradient, or a decreasing density gradient immediately after a peak. The disturbances were noted where visual observation of the discharge showed that a meniscus was present or where pronounced beam divergence occurred. This disturbance to the probe characteristic was of two forms and was always evident

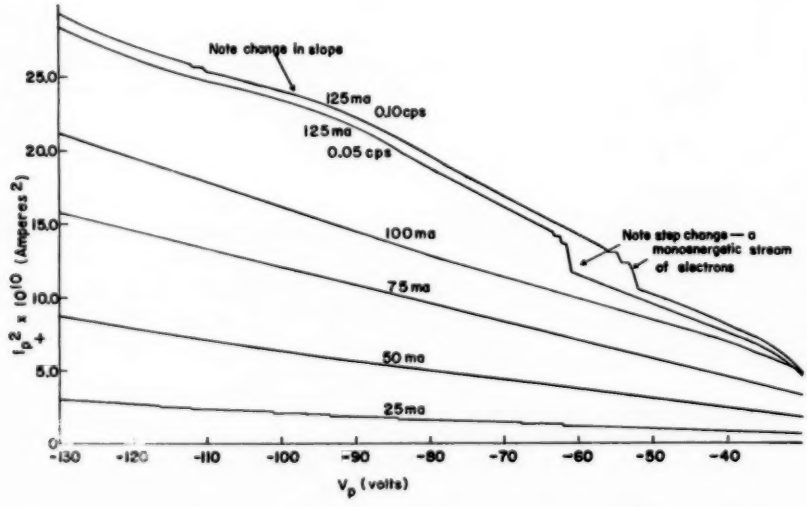

FIG. 2. Probe characteristic curve of ion current squared vs probe potential, showing high-energy electrons which one associated with the electron oscillations.

well into the ion-collecting region of the curve. The first form was a slight change in slope of the i_p vs V_p curve at about -100 volts with respect to the anode. The slope change became quite pronounced on the i_p^2 vs V_p plots. These slope changes seemed to be associated with a peak density gradient, and hence, in accord with the theory of Allis[4] predicting that oscillations are being initiated at such locations. The second form of disturbance (only observed at the highest discharge current, 125 ma) was a step increase in probe current at about -50 volts with respect to the anode, as well as the slope change at about -100 volts, as described above. An example of these disturbances is shown in Fig. 2.

Although in this case no frequency measurements were made to correlate with these disturbances, from the work of Emeleus and his group showing a correlation between oscillations and meniscus formation, it appears probable that the disturbances are caused by high-energy electrons produced as a result of electron oscillations in the interacting meniscus region of the discharge in which energy exchange is taking place between the beam electrons and the random plasma electrons.

It is suggested that the unmodulated beams of electrons, coming from the cathode, passing through and maintaining the plasma, suddenly become unstable and give rise to electron oscillations of the plasma in the presence of an associated decreasing plasma density gradient. In this interaction of beam and plasma electrons, electrons having energies of up to about 100 electron volts (well in excess of the tube voltage drop) are produced. The step-like disturbance at -50 volts is interpreted to be a monoenergetic group of electrons associated with a minimum of a density gradient and hence peak oscillation intensity.

*Work supported by the Office of Naval Research.

†Captain, United States Army.

[1]A. I. Akhiezer and Ya. B. Fainberg, J. Exptl. Theoret. Phys. (U.S.S.R.) 21, 1262 (1951); I. F. Kharchenko, Ya. B. Fainberg, P. M. Nikoleyev, et al., Proceedings of the Fourth International Conference on Ionization Phenomena in Gases (North Holland Publishing Company, Amsterdam, 1960), Vol. II, Chap. IIIB, pp. 671-680.

[2]D. P. Bohm and E. P. Gross, Phys. Rev. 75, 1851 (1949); 75, 1864 (1949).

[3]M. J. Druyvesteyn, Z. Physik 64, 790 (1930).

[4]W. P. Allis, Electronic Waveguides, Microwave Research Institute Symposium Series (Polytechnic Press, Brooklyn, 1959), Vol. VII, pp. 149-155.

[5]D. W. Mahaffey, G. C. McCullagh, A. Garscadden, and K. G. Emeleus, Proc. Roy. Irish Acad. (to be published).

LIFETIME EFFECTS IN CONDENSED FERMION SYSTEMS*

A. Bardasis and J. R. Schrieffer

Department of Physics, University of Illinois, Urbana, Illinois

(Received July 7, 1961)

It has been pointed out[1] that lifetime effects in the superconducting state can be of great importance in obtaining the excitation spectrum of the system. The concept of a clearly defined elementary excitation only has significance when the state is long lived; this condition is expressible by $E_1 \ll E_0$ where the energy of the excitation is $E = E_0 + iE_1$. The original[2] BCS theory of superconductivity obtains exact eigenstates for a reduced Hamiltonian which contains no damping effects. If one attempts to include finite-lifetime effects, a Green's function formulation of the problem provides a more convenient approach than the variational method used by BCS. This technique has been used by many workers, and we follow most closely the formulations of Nambu[3] and Eliashberg.[4]

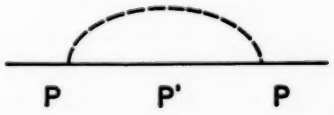

FIG. 1. Self-energy diagram used to evaluate the integral equation for the energy gap Δ_p.

Within these schemes, the evaluation of the self-energy diagram of Fig. 1 gives an integral equation for the energy gap $\Delta_{p'}$ at $T = 0°K$ as a function of the momentum-energy four-vector $p = (\vec{p}, p_0)$:

$$\Delta_p = -\int \frac{d^4p'}{(2\pi)^4} \frac{i}{(Z_{p'})^2} \frac{\Delta_{p'} V_{p'p}}{(p_0')^2 - [1/(Z_{p'})^2][(\epsilon_{p'})^2 + (\Delta_{p'})^2] + i\eta}. \quad (1)$$

$V_{p'p}$ is the two-body scattering potential, $\eta = 0^+$, and ϵ_p is the electron kinetic energy measured

from the Fermi surface. The quantity Z_p is given by $1-(\zeta_p/p_0)$, where ζ_p satisfies an integral equation similar to (1) and gives the normal state single-particle self-energy in the limit $\Delta_p \to 0$. The imaginary part of ζ_p gives rise to damping effects in the energy gap equation. If the potential $V_{p'p}$ is taken to be independent of p_0' and p_0, the analytic properties of the single-particle Green's function $G(p)$ allow us to reduce the integral equation to

$$\Delta_p = 2\,\mathrm{Im}\int\frac{d^3p'}{(2\pi)^3}V_{p'p}\int_0^\infty\frac{dp_0'}{(2\pi)}\frac{\Delta_{p'}/(Z_{p'})^2}{(p_0')^2-(\bar{E}_{p'})^2+i\eta}, \quad (2)$$

where we have set

$$(\bar{E}_{p'})^2=\frac{1}{(Z_{p'})^2}[(\epsilon_{p'})^2+(\Delta_{p'})^2]=(E_{p'}/Z_{p'})^2. \quad (3)$$

It is straightforward to generalize (2) to include potentials depending on p_0 and p_0'. Assuming that the analytic continuation of $G(p)$ into the lower half-plane for $p_0>0$ has a simple pole corresponding to an elementary excitation of energy

$$\bar{E}_{p'}{}^{r}=\bar{E}(\vec{p}',p_0')\Big|_{p_0'=\bar{E}_{p'}{}^{r}}, \quad (4)$$

the integral equation becomes

$$\Delta_p=-\mathrm{Re}\int\frac{d^3p'}{(2\pi)^3}V_{p'p}\frac{\Delta(p',\bar{E}_{p'}{}^{r})}{2Z_{p'}E_{p'}\{1-E_{p'}[\partial(1/Z_{p'})/\partial p_0']\}_{p_0'=\bar{E}_{p'}{}^{r}}}. \quad (5)$$

As we have noted previously, the damping effects are contained in the quantity $Z_p=1-(\zeta_p/p_0)$. When Z_p is set equal to unity, the integrand becomes real and the equation reduces to that of BCS. In our calculation, we investigate the effect of damping on the integral equation by considering various forms of the function ζ_p. The real part of ζ_p may be incorporated in a renormalization of the real excitation energies ϵ_p, so that we need only include $\mathrm{Im}\zeta_p$ in Z_p. We consider a general form for Z_p in which the damping is proportional to a power of p_0: i.e.,

$$Z_p=1+\frac{i\alpha|p_0|^n\,\mathrm{sgn}(p_0)}{p_0}. \quad (6)$$

With this form for Z_p, the energy gap equation becomes

$$\Delta_p=-\int\frac{d^3p'}{(2\pi)^3}V_{p'p}\frac{\Delta_{p'}}{2E_{p'}[1+n^2\alpha^2|p_0'|^{2(n-1)}]}, \quad (7)$$

where $p_0'=\bar{E}_{p'}{}^{r}$. We will consider the three cases $n=0$, 1, 2. It should be noted here that our assumed form for $\mathrm{Im}\zeta_p$ is not entirely satisfactory since this quantity must vanish for $|p_0|<\Delta_p$. Therefore, in the $n=0$ case we may only consider the $\Delta_p\to 0$ situation. For $n=1$, the approximation is much better, and for the important case where $n=2$, the error introduced is completely negligible.

(1) $n=0$. The $n=0$ case corresponds to constant damping. For the two-body interaction $V_{p'p}$, we consider a separable potential of the form

$$V_{p'p}=-V, \quad |\epsilon_{p'}|,|\epsilon_p|<\hbar\omega_0, \quad (8)$$

$$V_{p'p}=0, \text{ otherwise.}$$

With $n=0$, setting $\Delta_p=0$ in the integral equation (7) allows us to determine the minimum value of α such that no transition to the superconducting state occurs; i.e., $T_c=0°\mathrm{K}$. We find $\alpha_c=\hbar\omega_0\times\exp[-1/N(0)V]$, where $N(0)$ is the density of electron states of one spin at the Fermi surface. This result agrees with that of Suhl.[5]

(2) $n=1$. The separable potential of case (1) gives the gap equation

$$\frac{1}{N(0)V}=\int_0^{\hbar\omega_0}\frac{d\epsilon}{(\epsilon^2+\Delta^2)^{1/2}}\frac{1}{(1+\alpha^2)}.$$

The solution is of the BCS type with $\Delta_p=\hbar\omega_0/\sinh[(1+\alpha^2)/N(0)V]$ for $|\epsilon_p|\le\hbar\omega_0$ and $\Delta_p=0$ otherwise. Thus, the inclusion of linear damping modifies the BCS solution only through the introduction of a reduced effective coupling constant $N(0)V/(1+\alpha^2)$.

(3) $n=2$. The $n=2$ case is of interest both for superconductors and He^3 in which a short-range potential gives rise to damping by exciting particles out of the Fermi sea. For quadratic damping, the $T=0°\mathrm{K}$ gap equation is

$$\Delta_p=-\int d^3p'\frac{\Delta_{p'}V_{p'p}}{[(\epsilon_{p'})^2+(\Delta_{p'})^2]^{1/2}\{2[1+4\alpha^2((\epsilon_{p'})^2+(\Delta_{p'})^2)]^{1/2}-1\}}. \quad (9)$$

In the case of the superconductor the screened Coulomb interaction leads to α of the order $1/5E_F$, indicating that Coulomb damping effects are small since matrix elements of $V_{p'p}$ for excitations from the Fermi surface of energy $5E_F$ are small.

For He^3, damping effects are important in determining Δ_p and the transition temperature to a possible superfluid state. Due to the hard-core potential the integral equation must be solved in coordinate space. However, we can obtain an estimate for the reduction of T_c due to damping effects by considering an effective separable potential. The coefficient α can be estimated from the thermal conductivity data of Anderson, Salinger, and Wheatley.[6] We find $\alpha = 9.1\times10^{16}$ erg^{-1}. When compared to the He^3 Fermi temperature of about 3°K, $\alpha = 37.6E_F^{-1}$, indicating that the imaginary and real parts of the excitation energy are equal at $p_0 \simeq E_F/40$. With the separable potential, the transition temperature T_c is given by

$$\frac{1}{N(0)V}=\int_0^{\hbar\omega_0} d\epsilon \frac{\tanh(\beta_c\epsilon/2)}{\epsilon[2(1+4\alpha^2\epsilon^2)^{1/2}-1]}, \qquad (10)$$

where $\beta_c = kT_c$. Choosing $\hbar\omega_0 \simeq E_F$, V is determined by requiring T_c in the absence of damping to be T_c^0 calculated by Emery and Sessler.[7] The critical temperature T_c in the presence of damping is found to be $T_c = 0.016\,T_c^0 \simeq 8\times10^{-4}$°K. Thus it appears that the effects of damping account for the absence of a transition to a superfluid state in current experiments performed at temperatures $T \geq 5\times10^{-3}$°K.

---

*This work was supported in part by the Air Force Office of Scientific Research. One of the authors (A. B.) was aided by a fellowship from Texas Instruments, Inc.

[1]J. Bardeen, Superconductivity Conference, Cambridge, 1959 (unpublished).

[2]J. Bardeen, L. N. Cooper, and J. R. Schrieffer, Phys. Rev. 108, 1175 (1957).

[3]Y. Nambu, Phys. Rev. 117, 648 (1960).

[4]G. M. Eliashberg, J. Exptl. Theoret. Phys. U.S.S.R. 38, 966 (1960) [translation: Soviet Phys.-JETP 11, 696 (1960)].

[5]H. Suhl, Bull. Am. Phys. Soc. 6, 119 (1961).

[6]A. C. Anderson, G. L. Salinger, and J. C. Wheatley, Phys. Rev. Letters 6, 443 (1961).

[7]V. J. Emery and A. M. Sessler, Phys. Rev. 119, 43 (1960).

PERSISTENT RING CURRENTS IN AN IDEAL BOSE GAS

J. M. Blatt

Bell Telephone Laboratories, Murray Hill, New Jersey, and
Department of Applied Mathematics, University of New South Wales, Kensington, N. S. W., Australia
(Received July 10, 1961)

In their fundamental paper on the theory of electrical resistivity, Kohn and Luttinger[1] considered a gas of particles which do not interact with each other, but do interact with randomly located scattering centers. They proved that this system has a normal electrical resistivity, and that the statistics (Fermi-Dirac or Bose-Einstein) of the particles does not make any qualitative difference.

Their proof breaks down, however, below the Bose-Einstein condensation point, where one single-particle quantum state is occupied by a macroscopic number of particles. We have investigated this case for a system contained in a ring-shaped volume, and find that persistent ring currents are set up by the usual method. That is, the ring is placed between the poles of a magnet, then cooled below the Bose-Einstein transition temperature, and finally removed from the external magnetic field. Within the assumptions of the model, the lifetime of these currents is infinite, independently of the physical size of the ring.

The phenomenology corresponding to this model is similar to, but not identical with, the London[2] equations. In particular, the "flux quantum" hc/e enters the equations explicitly. If the "bosons" are taken to be electron pairs,[3] the charge e is twice the electronic charge. The relation between the flux Φ through the ring, and the "external" flux Φ_e, is given in the model by

$$\Phi - m\Phi_1 = (\Phi_e - m\Phi_1)/(1+qN_0). \qquad (1)$$

Here Φ_1 is the "flux quantum," m is the integer closest to the ratio Φ_e/Φ_1 at the time the system is cooled through the transition temperature, N_0 is the number of condensed bosons (electron pairs), and q is the quantity

$$q = e^2 \mathfrak{L}/(2\pi\rho)^2 M, \qquad (2)$$

where $\mathfrak{L}$ is the self-inductance of the ring, ρ is its mean radius, and e and M are the charge and mass of the boson. In applications to superconductors, e and M should be taken as twice the charge and mass of an electron, respectively, and in the limit of low temperatures, N_0 is half the number of conduction electrons in the sample.

As the ring is cooled down through the transition temperature, without being moved, Φ_e remains constant, but small ring currents are generated which make the actual flux Φ very close to an integral number of flux units, $m\Phi_1$.[4] When the ring is then pulled out of the external magnetic field, Φ_e decreases to zero, and Eq. (1) predicts a new value for the final flux Φ maintained by the persistent currents. This final flux may differ appreciably from an integral number of flux "quanta," the difference being given by

$$(\Phi - m\Phi_1)/\Phi_1 = -m/(1+qN_0). \qquad (3)$$

With the experimental conditions of reference 4, m is of order unity and qN_0 much larger than 1; thus quantization should be maintained. But it should be possible to construct experimental conditions so as to observe the predicted deviation (3).

It is well known[3] that the Meissner effect in actual superconductors can be understood in precise analogy to such a Bose-Einstein gas model, the "bosons" being attractively correlated electron pairs. It seems likely, therefore, that the model calculation of persistent currents reported here can also be extended to an appropriate calculation for actual superconductors. There are, of course, significant differences between this model and actual superconductors, the most important difference being the complete absence, in the model, of an energy gap. We conclude that an energy gap is not required for the understanding of persistent currents; for if it were, we would not have been able to obtain persistent currents in the model.

The strictly infinite lifetime of ring currents in this model can be traced directly to difficulties in the foundations of nonequilibrium statistical mechanics[5]; these difficulties are present in the Kohn-Luttinger theory, but are concealed in this theory by the extensive averaging necessary at high temperatures.

The author is grateful to Dr. P. W. Anderson, Dr. L. M. Delves, and Dr. R. Garwin for valuable and illuminating discussions, and to Bell Telephone Laboratories for a visit in the course of

which many of these ideas were conceived.

[1]W. Kohn and J. M. Luttinger, Phys. Rev. 108, 590 (1957).
[2]F. London, Superfluids (John Wiley & Sons, New York, 1950), Vol. 1.
[3]J. M. Blatt, Progr. Theoret. Phys. (Kyoto) 24, 851 (1960).
[4]After completion of this work, the author received a preprint by Deaver and Fairbank, reporting this very effect [B. S. Deaver, Jr., and W. M. Fairbank, Phys. Rev. Letters 7, 43 (1961)].
[5]J. M. Blatt, Progr. Theoret. Phys. (Kyoto) 22, 745 (1959).

MILLIMETER CYCLOTRON RESONANCE EXPERIMENTS IN DIAMOND

Conrad J. Rauch
Lincoln Laboratory,* Massachusetts Institute of Technology, Lexington, Massachusetts
(Received June 29, 1961)

Cyclotron resonance has been observed in several semiconducting diamonds at 70 kMc/sec and at helium temperatures. For magnetic fields below 33.5 kilo-oersteds, two strong lines have been observed having effective masses of $(0.70 \pm 0.01)m_0$ and $(1.06 \pm 0.04)m_0$ with little or no anisotropy. The experiments will be described in this Letter.

The 4-mm wave spectrometer system is similar to a 2-mm spectrometer described previously,[1] with the following exceptions. A three-port circulator[2] and a commercial 1N2792 crystal detector are used to observe the signal reflected from the microwave cavity which operates in the TM_{013} mode and has a loaded Q factor of about 1500. As previously, the samples are positioned in the high axial electric field of the cavity for cyclotron resonance. The static magnetic field is obtained from a commercial 12-inch electromagnet with a 9/16-inch pole face gap. The light modulation of carriers and detection system as described previously is used.

The diamond crystals which were investigated are of the IIb variety.[3] Resonance was observed in only a few of the samples, and there appears to be a qualitative agreement of crystal perfection as determined from x-ray data with the observed linewidths in the spectrum. Some samples having $\omega\tau$ less than unity exhibited the characteristic nonresonant microwave magnetoresistance. Figure 1 shows a typical experimental trace in one of the better samples.

The curve is a reproduction of a recorder trace of the absorption at 69.2 kMc/sec as a function of magnetic field. The data were obtained at an ~0.1-microwatt rf power level at 1.2°K with a low level of light excitation. Lines are observed at $0.70m_0$ and at $1.07m_0$ having linewidths given by $\omega\tau \approx 13$ and $\omega\tau \approx 7$, respectively. The recorder trace of absorption is taken as a linear function of magnet current but the magnetic field is linear only through the low-field line. The high-field line falsely appears to be asymmetrical and much broader than twice the low-field line, but this results from a progressive increase in nonlinearity of the magnetic field.

Absorption line intensities decrease upon moving the sample to a region of weaker rf electric field, thus indicating that cyclotron rather than paramagnetic resonance is observed. Detailed anisotropy measurements indicate that little or no anisotropy exists in either resonance within the limits of accuracy of the experiment. At 4.2°K, the spectrum below 33.5 kilo-oersteds is very similar with the exception of unresolved structure on the low-field side of the low-mass line. On occasion at relatively low rf level, both at 4.2°K and 1.2°K, a weak line at about $0.5m_0$ is observed which may be a "quantum effect" line.

An attempt to observe resonance in the conduction band by exciting carriers across the gap (5.5 ev) with a hydrogen arc has not been successful.

The carriers which are observed have been excited with a tungsten light source which does not visibly glow, thus suggesting that the resonances are due to carriers in the valence band since the

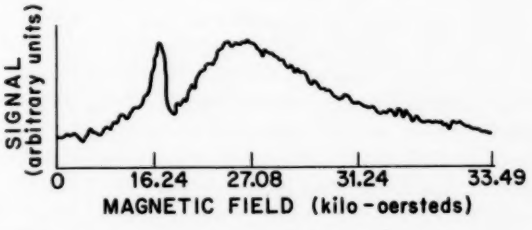

FIG. 1. Experimental trace of cyclotron resonance absorption in diamond at 69.2 kMc/sec and 1.2°K.

impurity levels in the IIb's lie a few tenths of a volt above the valence band.[4] An estimate of the spin-orbit splitting Δ of the order of 0.005 volt from atomic data suggests that possibly the constant-energy surfaces cannot be simply expressed by[5]

$$E(k)=Ak^2\pm[B^2k^4+C^2(k_x^2k_y^2+k_y^2k_z^2+k_z^2k_x^2)]^{1/2},$$

which is good for the valence band of germanium[6] and silicon,[7] but that higher order terms must be taken into account in the secular determinant for diamond. It has been suggested[8] that the low-mass line is due to the light hole, and that the high-mass line, being isotropic, is a spherical energy surface which goes with the split-off band, and that the heavy hole should be anisotropic and have a mass of $\sim 3m_0$. Further experiments are in progress to clarify the data.

Thanks are due to Dr. J. F. H. Custers of the Diamond Research Laboratory, Johannesburg, for providing the variety of samples. R. N. Dexter of the University of Wisconsin participated in a portion of the experiments. The continued interest and many invaluable discussions with H. J. Zeiger are gratefully acknowledged. W. C. Kernan and F. H. Perry assisted in making the measurements.

*Operated with support from the U. S. Army, Navy, and Air Force.

[1]C. J. Rauch, J. J. Stickler, H. J. Zeiger, and G. S. Heller, Phys. Rev. Letters 4, 64 (1960).

[2]J. B. Thaxter and G. S. Heller, Proc. Inst. Radio Engrs. 48, 110 (1960).

[3]For explanation of this nomenclature, see for example, E. W. Mitchell, J. Chem. Phys. Solids 8, 444 (1958).

[4]P. T. Wedepohl, Proc. Phys. Soc. (London) B70, 177 (1957); A. Halperin and J. Nahum, J. Phys. Chem. Solids 18, 297 (1961).

[5]G. Dresselhaus, A. F. Kip, and C. Kittel, Phys. Rev. 95, 568 (1954).

[6]R. N. Dexter, H. J. Zeiger, and B. Lax, Phys. Rev. 95, 557 (1954).

[7]R. N. Dexter and B. Lax, Phys. Rev. 96, 223 (1954).

[8]H. J. Zeiger and G. F. Dresselhaus (private communication).

ELECTRIC-FIELD-INDUCED MODULATION OF THE ABSORPTION DUE TO INTERBAND TRANSITIONS OF FREE HOLES IN GERMANIUM

M. A. C. S. Brown and E. G. S. Paige

Physics Department, Royal Radar Establishment, Malvern, England

(Reveived June 2, 1961)

Provided the structure of the valence band of Ge in the vicinity of $\vec{k}=0$ is independent of temperature, then the absorption due to direct interband transitions[1-3] depends on temperature only through the distribution function of the free holes. The distribution function is of prime importance in determining the absorption, and any agency which changes the energy distribution of holes in $\vec{k}$ space will produce a corresponding change in absorption. It is possible, therefore, to study the effect of a high electric field (E) on the distribution function in a direct manner. In principle, if the details of the band structure are known, it is possible to relate a photon energy with a range (because of warping) of $\vec{k}$ for both types of hole and hence to obtain the distribution function in $\vec{k}$ space of both light and heavy holes. Such a relationship is shown in Fig. 1 for transitions to the split-off band, for a band structure calculated as described below. The arrows indicate the value of k^2 at which the energy of the hole (light or heavy according to band) is $\frac{3}{2}kT$.

In practice the change in absorption was observed due to a change in distribution produced by the high field; such a differential method is inherently more sensitive than a method measuring the total absorption. In a subsidiary experiment performed for the purpose of comparison, the distribution function was changed in a known way by raising the lattice temperature a small amount and the change in absorption observed (to be referred to as the δT effect). The change in absorption can be calculated from Kane's[3] theory. Taking the spin-orbit splitting as 0.290 ev, and the other band-structure parameters as given by Kane—but modifying the energy dependence on $\vec{k}$ of the split-off band by 30%, as Kane suggests, crudely to allow for higher order perturbation terms not rigorously included—the change in absorption due to a 13.5% increase of temperature of a Maxwellian distribution at 93°K (Fig. 1, curve 1) and 293°K (Fig. 2, curve 1) has

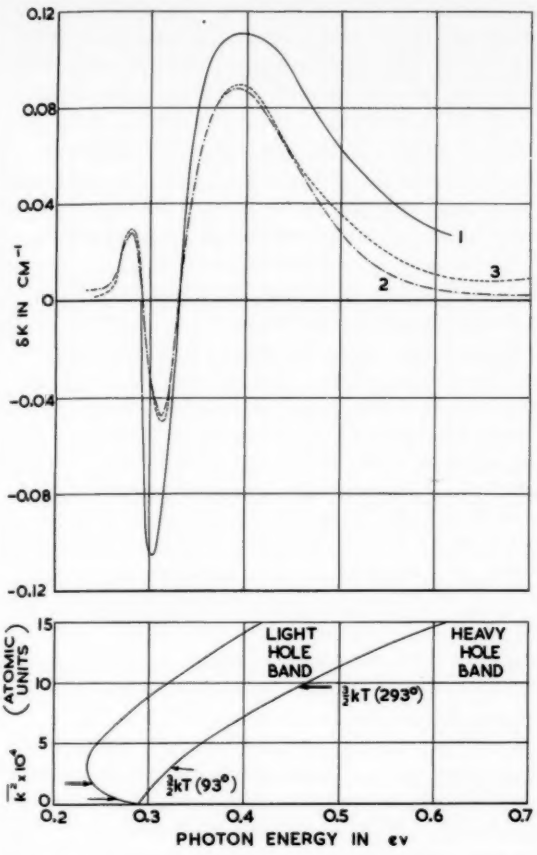

FIG. 1. Change in absorption with photon energy for a lattice temperature of 93°K. Curve 1, theoretical δK for transitions between heavy-hole and split-off band ($\delta T/T = 0.135$). Curve 2, field effect for $E = 170$ v cm^{-1}. Curve 3, δT effect for $\delta T = 12.6$°K. Below, the relationship between k^2 and photon energy.

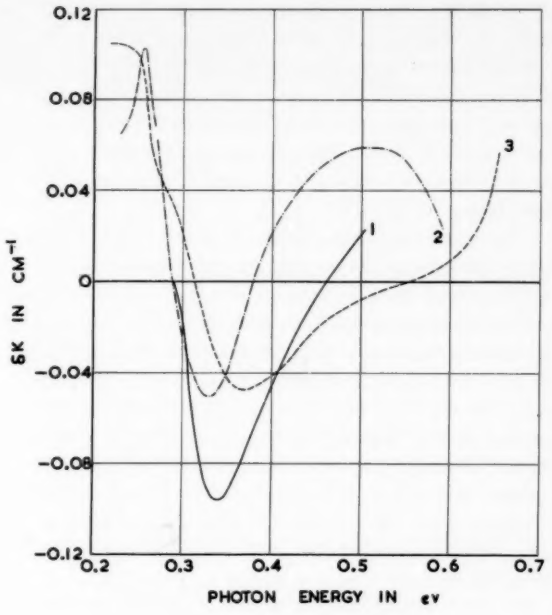

FIG. 2. Change in absorption with photon energy for a lattice temperature of 293°K. Curve 1, theoretical δK for transitions between heavy-hole and split-off band ($\delta T/T = 0.135$). Curve 2, $\delta K \times 5$ for field effect at $E = 1480$ v cm^{-1}. Curve 3, $\delta K \times 3$ for δT effect, $\delta T = 13$°K.

been calculated for transitions from the heavy-hole band to the split-off band. (The free carrier concentration was chosen to be 4.4×10^{15} cm^{-3}.)

In the experimental arrangement for measuring the field effect, light from a tungsten filament lamp was passed through a germanium filter (to prevent optical excitation of carriers in the specimen) and focussed on the optically polished germanium specimen mounted in a low-temperature cell. After being passed through a Leiss spectrometer, the light was finally focussed on a cooled (77°K) InSb detector. High-field pulses of 5-μsec duration and of repetition frequency 1.3 sec^{-1} were applied to the dumbbell-ended specimen. Though it caused a significant rise in lattice temperature, a pulse of 5-μsec duration was necessary to enable a saturation of the field effect to be observed since the time constant of the detector was 1 μsec. However, it was always possible to distinguish and eliminate thermal effects because of the relatively long thermal time constant of the specimen. Determination of the total intensity of the light transmitted enable the change in absorption (δK) to be calculated.

The subsidiary experiment was performed using the same optical arrangement. The change in lattice temperature was produced by passing a direct current through the specimen for 2 sec. A steady state was reached during this period, the temperature increase being indicated by a thermocouple of suitable response time and in good thermal contact with the specimen. The beam was stopped down so that only a volume of the crystal close to the thermocouple was "active."

Measurements have been made at various lattice temperatures between 90°K and 320°K on a p-type Ge sample containing 4.4×10^{15} cm^{-3} free carriers. Curve 2 of Fig. 1 shows δK for a field of 170 v cm^{-1} and curve 3 shows the δT effect for

$\delta T/T = 0.135$, both measured with the lattice at 93°K. A similar pair of results are shown in Fig. 2 for a lattice temperature of 293°K. The change of absorption due to transitions of heavy holes to the split-off band can readily be identified by comparison with the calculated curve; a maximum at about 0.27 ev is associated with transition of the light holes.

Some of the salient points which emerge from these results and from the velocity field curves for the same sample are:

(1) At a lattice temperature of 93°K, a comparison between the field effect and the δT effect shows that in electric fields up to 350 v cm^{-1} the distribution remains Maxwellian, within the accuracy of the measurement. Figure 3 shows the relationship between δT and E obtained from the comparison. The calculated change in absorption of heavy holes is in reasonable agreement with the observed values both with regard to shape and magnitude.

(2) At a lattice temperature of 293°K there is a marked difference between the field effect, the δT effect, and the computed δK. If the low-temperature band-structure parameters are correct, then it is possible that the discrepancy between the predicted curve and the δT effect may be due (a) to changes of the band structure with temperature to which the calculated and observed results are sensitive, or (b) to indirect transitions. Alternative (a) is favored since for indirect transitions $\delta K_{ind}/\delta T$ is always positive, and δK_{ind} has been estimated to be less than 20% of the value for direct transitions. In an electric field the departure of the distribution from Maxwellian at this higher lattice temperature can be understood since the cross section for hole-hole scattering falls[4] while the cross section for phonon scattering rises with increasing temperature.

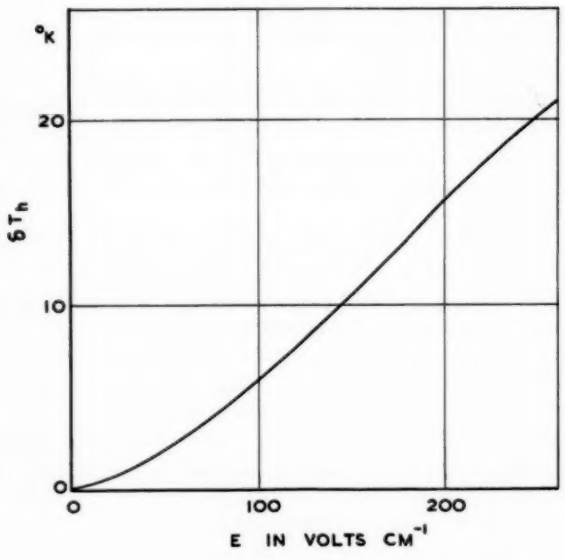

FIG. 3. The increment of hole temperature with electric field strength for a lattice temperature of 93°K. Maximum error in δT is ±15%.

(3) For given scattering mechanisms, Fig. 3 enables the field dependence of the mobility to be predicted and, from the energy balance equation, a value of $(\Xi_{lop}/\Xi_{lac})^2$ can be determined if the same value is assumed for all transitions. Taking Brown and Bray's[5] values of the parameters, which occur in the mobility formula, we find (i) that the calculated ratio of zero-field mobilities at 93°K and 293°K agrees with the observed ratio to within 4%; (ii) that a dependence of lattice mobility, μ_L, on the hole temperature, T_h, of $\mu_L \propto T_h^{-\delta}$, $\delta \sim 1.3$, has to be assumed to account for the observed dependence of mobility on field; and (iii) that the mean value of $(\Xi_{lop}/\Xi_{lac})^2$ is 1.6 ± 0.3, which is approximately half the value required if optical and acoustical phonon scattering are responsible for the $\mu_L \propto T^{-2.3}$ law, and implies that the normal form of optical and acoustical phonon scattering is not entirely responsible for the high value of δ. (Calculations we have made show that the nonparabolic shape of the light-hole band[3] makes an insignificant contribution to the temperature dependence of μ_L.)

In conclusion we should like to point out that the theoretical response time of the modulation is the energy relaxation time τ_ϵ of the free holes. At room temperature $\tau_\epsilon \sim 10^{-11}$ sec,[6] and is not more than 10^{-10} sec at 93°K. Since substantial depths of modulation (>10%) can be achieved with the lattice at 93°K, the field effect we observe could form the basis of a modulator capable of modulating a light beam at very high frequencies.

[1]W. Kaiser, R. J. Collins, and H. Y. Fan, Phys. Rev. 91, 1380 (1953).

[2]A. M. Kahn, Phys. Rev. 97, 1647 (1955).

[3]E. O. Kane, J. Phys. Chem. Solids 1, 82 (1956).

[4]T. P. McLean and E. G. S. Paige, J. Phys. Chem. Solids 16, 220 (1960).

[5]D. M. Brown and R. Bray, Proceedings of the International Semiconductor Conference, Prague, 1960 (to be published). These authors have also observed similar modulation effects at low temperature to those reported here.

[6]A. F. Gibson, J. W. Granville, and E. G. S. Paige, J. Phys. Chem. Solids (to be published).

HOT ELECTRON EMISSION FROM SILICON *pn* JUNCTIONS PARALLEL TO THE SURFACE*

J. L. Moll, N. I. Meyer,† and D. J. Bartelink
Solid-State Electronics Laboratories, Stanford University, Stanford, California
(Received June 19, 1961)

A number of papers have been published on emission of electrons from semiconductor *pn* junctions into vacuum.[1-6] It is a common feature of these works that the emitted electrons have come from regions where the junction intersected the surface. This emission geometry limits the magnitude of the emitted current and makes a quantitative interpretation of the experimental results difficult. An attempt to observe emission from a *pn* junction parallel to the emitting surface was mentioned by one of the authors.[4] The attempt did not succeed—apparently because the neutral *n* layer between the junction and the emitting surface was too thick (~1400 A).

In this Letter we present some results on electron emission from silicon *pn* junctions parallel to the emitting surface. The junctions are made from cubes of 0.02 ohm cm *p*-type silicon approximately one millimeter on the edge. Four faces were diffused with thick *n*+ regions whose purpose was to make contact to one face on which a thin *n*-type region was diffused. The thin layer was about 1000 A thick. One face was used to contact the *p*-type body, thus allowing bias to be applied to the junction. Typical breakdown voltages were 10 volts for the thick junction and 4.5 to 6 volts for the thin junction.

The emission current was measured in a demountable vacuum system with the device positioned at the center of a hemispherical collector. A small hole was drilled in the collector to allow light to be shone on the emitting surface. At prebreakdown reverse bias voltages the junction current was typically raised from about 50 μa to 1 ma by the light. The emission current due to these photoelectrons is called photoenhanced emission current. Without the light, the junction voltage had to be raised to the breakdown region in order to give rise to a measurable emission current with the sensitivity available (~10^{-14} amp). Prior to each measurement the junctions were etched in HF acid to remove silica and placed in the vacuum system without exposure to air.

A method was developed for thinning down the *n* region in well-defined steps. It consists of growing layers of SiO_2 on the crystal in boiling water. The SiO_2 layer is subsequently removed by etching in HF. The rate of removal was calibrated on uniformly doped silicon crystals by a weighing technique and was found to attain a value of about 34 A per boiling. This is a convenient value with a view to constructing the emission devices. When the boiling water technique was applied to crystals with a *pn* junction close to the surface, it was found that the rate of removal was reduced to about 5 A per boiling when the surface came to within about 200 A of the field region of the *pn* junction.

The emission current is shown in Fig. 1 as a function of the number of boiling water, HF steps and is seen to increase exponentially with amount of material removed. The exponential increase levels off between 18 to 25 steps of boiling. This is interpreted as being due to the reduction in the rate of removal as discussed above.

Due to the relatively simple geometry it has been possible to set up a mathematical model of the device and to derive theoretical expressions for the emitted electron current. The theoretical results are based on an approximate solution of Boltzmann's transport equation taking into account the important types of interaction between the hot electrons and the crystal lattice.[7] These interactions are scattering by optical phonons and secondary ionization. The theoretical expressions include some basic parameters describing these interaction processes. The values of the interaction parameters are presently subject to controversial discussions.[8] Analysis of our experimental results seems to resolve some of the questions concerning the appropriate values to be used for the interaction parameters.

The energy distribution of the hot electrons after they have been accelerated in the strong field of the *pn* junction and subsequently diffused to the emitting surface through the neutral region is mainly determined by the following quantities:

The field E in the *pn* junction, the width w of the *pn* junction, the thickness L of the neutral region, the mean free path l_γ for optical phonon scattering, the mean free path l_i for ionization, the energy $\mathcal{E}_\gamma$ of the optical phonons, and the threshold energy $\mathcal{E}_i$ for ionization. The parameters E, w, and L may be varied independently (within certain limits) by choosing the appropriate device parameters (doping levels, impurity profile, etc.). The quantities l_γ, l_i, $\mathcal{E}_\gamma$,

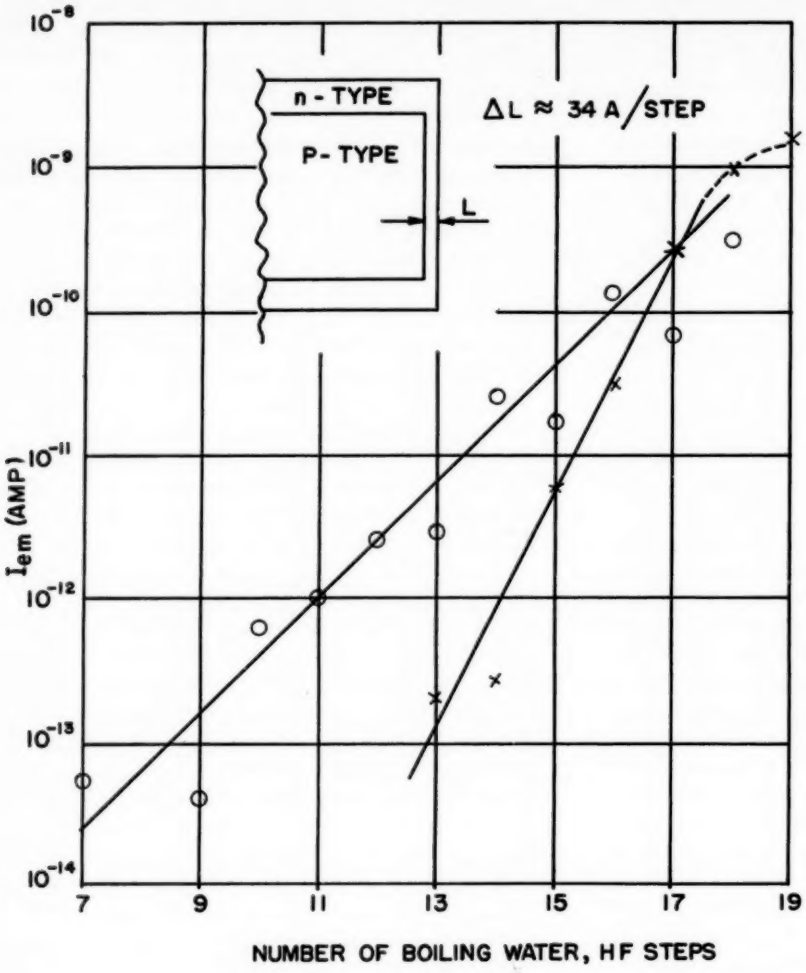

FIG. 1. Emission current as a function of the number of boiling water, HF steps. Each step removes about 34 A of silicon. The applied junction voltage is 6 volts. No light was shone on the junction. o: measured on sample No. 8: ×: measured on sample No. 6.

and $\mathcal{E}_i$ are characteristic of the material in question. For silicon $\mathcal{E}_\gamma = 0.063$ ev as found by neutron diffraction experiments.[9] The values of the remaining three parameters are subject to discussion as mentioned above.

The magnitude of the emitted current depends in addition to the above parameters on the electron affinity $\mathcal{E}_{sf}$. The value of $\mathcal{E}_{sf}$ has been determined from the retarding potential measurements for an untreated silicon surface.

The values of $\mathcal{E}_i$, l_γ, and l_i enter into the theory in a manner such that one single measurement can be fitted by a wide range of values. However, by considering retarding field measurements, variation of current with thickness, and total current, it is possible to narrow down the possible range of values.

The theoretical treatment gives the following dependence[7] of emission current on L:

$$I_{em} \sim \exp(-L/\lambda), \tag{1}$$

where

$$\lambda = l_i \left\{ 3\left(1+\frac{l_i}{l_\gamma}\right)\left[1+\left(1+\frac{l_i}{l_\gamma}\right)\left[1+\left(1+\frac{4l_\gamma}{l_i+l_\gamma}\frac{kT_{e1}}{\mathcal{E}_\gamma}\right)^{1/2}\right]\frac{\mathcal{E}_\gamma}{2kT_{e1}}\right]\right\}^{-1/2}, \tag{2}$$

and T_{e1} is an equivalent temperature describing the energy distribution of the electrons with energies less than $\mathcal{E}_i$ at the end of the field region. The values of λ found from Fig. 1 are $\lambda_1 = 20$ A and $\lambda_2 = 35$ A. For the two extreme theories discussed by Shockley,[8] we find the following limits for l_i by using the above experimental values for λ together with the theoretical expression (2):

$$35 \text{ A} < l_i < 60 \text{ A for } l_i \ll l_\gamma; \quad (3)$$

$$300 \text{ A} < l_i < 500 \text{ A for } l_i = 18 l_\gamma,$$

$$\text{hence } 16 \text{ A} < l_\gamma < 28 \text{ A}. \quad (4)$$

The first case corresponds to the results of Wolff[10] and others, while the second case corresponds to Shockley's theory.[8]

Figure 2 shows the results of a retarding potential experiment. From the value of the cutoff voltage V_{cm}, the electron affinity has been determined from

$$\mathcal{E}_{sf} \approx \mathcal{E}_g + qV_{appl} - qV_{cm} \approx 3.7 \text{ ev}, \quad (5)$$

since the built-in potential is approximately equal to the energy gap $\mathcal{E}_g$ for the junctions in question.

It is found theoretically that the high-energy part of the distribution function is approximately Maxwellian with an effective temperature:

$$T_{e2} = 2T_{e1} \Big/ \left\{ \frac{l_\gamma + l_i}{l_i} \left[1 + \left(1 + 4 \frac{l_\gamma}{l_\gamma + l_i} \frac{kT_{e1}}{\mathcal{E}_\gamma} \right)^{1/2} \right] \right\}. \quad (6)$$

The value found from Fig. 2 is $T_{e2} \approx 0.5$ volt.

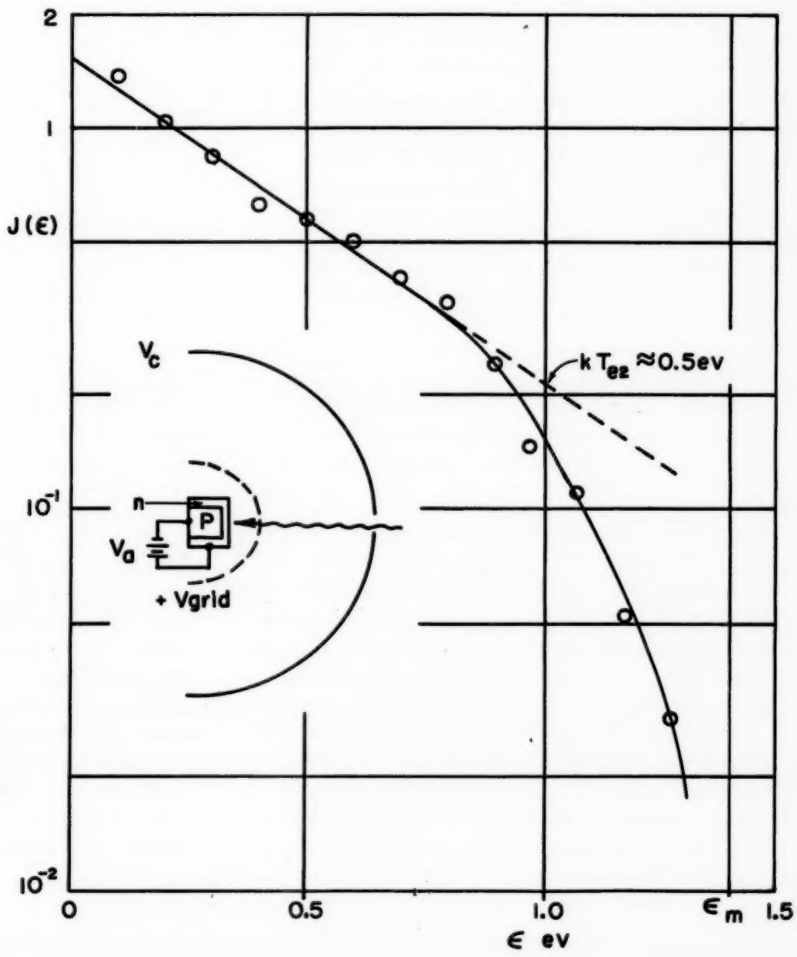

FIG. 2. Photoenhanced emission current as a function of energy. $J(\mathcal{E})$ is the contribution to the emitted current from electrons with energies between $\mathcal{E}$ and $\mathcal{E} + d\mathcal{E}$ (measured in arbitrary units). The result is obtained by differentiating an experimental curve for the magnitude of the total emitted current as a function of the applied retarding potential. The reverse junction bias is $V_{appl} = 4$ volts.

Using the values from (3) together with (6) gives rise to a value of T_{e2} which is an order of magnitude too small. For the values in (4), T_{e2} comes out about a factor of two too small.

Finally, the experimental value of the total emitted current was compared to the theoretical results. Using the values in (3), the calculated emission current was found to be several orders of magnitude smaller than the measured current. The same applies to the theoretical emission current corresponding to the lower limit in (4) while the upper limit gave reasonable agreement between calculated and measured results. If we assume a smaller ratio of l_i/l_γ than 18, all of the data can be fitted with $l_i \approx 100$ A and $l_\gamma \approx 50$ A. One of these parameters can be changed by $\pm 50\%$ and a fit still obtained by adjusting the other one. As l_i is increased, l_γ must be decreased to retain the fit.

It is concluded that the low values of l_i postulated by Wolff and others are not consistent with our results. The actual result does not satisfy either Shockley's assumption that $l_i \gg l_\gamma$ or Wolff's assumption that $l_\gamma \gg l_i$, but seems to favor Shockley's picture. There is an inherent experimental error in the retarding potential measurement in that the potential across the emitting face may vary by a few tenths of a volt giving too high a value for T_{e2}. If T_{e2} is reduced by a factor of 2, Shockley's picture fits fairly well but with a surprisingly small mean free path for optical phonon excitation. It would be of great interest to study the electrons which have lower energies than the 3.7 ev corresponding to the electron affinity of the untreated silicon surface. This may be accomplished, e.g., by coating the surface by Cs and thereby lowering $\mathcal{E}_{sf}$. Preliminary results on devices of the type described above with a Cs layer on the surface have been obtained. The value of $\mathcal{E}_{sf}$ was about 1.8 ev and the maximum emission current was 0.02 μa. No detailed comparison with theory has been made so far, as it is believed that the magnitude of the emission current is influenced by the presence of an oxide layer between the silicon and the Cs layer.

*Work supported by the Signal Corps.

†On leave from the Technical University of Denmark, Copenhagen, Denmark.

[1]J. A. Burton, Phys. Rev. 108, 1342 (1957).
[2]J. Tauc, Nature 181, 38 (1958).
[3]W. E. Spicer, Bull. Am. Phys. Soc. 5, 69 (1960).
[4]B. Senitzky, Phys. Rev. 116, 874 (1959).
[5]L. Patrick and W. J. Choyke, Phys. Rev. Letters 2, 48 (1959).
[6]R. E. Simon and W. E. Spicer, J. Appl. Phys. 31, 1505 (1960).
[7]J. L. Moll, N. I. Meyer, and D. J. Bartelink (to be published).
[8]W. Shockley, Solid-State Electronics 2, 35 (1961).
[9]B. N. Brockhouse, Phys. Rev. Letters 2, 256 (1959).
[10]P. A. Wolff, Phys. Rev. 95, 1415 (1954).

LINEAR EFFECT OF APPLIED ELECTRIC FIELD ON MAGNETIC HYPERFINE INTERACTION

N. Bloembergen
Harvard University, Cambridge, Massachusetts
(Received July 10, 1961)

It has been shown that an electric field will change the quadrupole coupling of a nucleus which is not at a center of inversion symmetry.[1-3] The purpose of this note is to show that the magnetic hyperfine interactions, either isotropic or anisotropic, can also be linear functions of the applied electric field. Consider first the isotropic or contact interaction $A\vec{I}\cdot\vec{S}$. The variation in the scalar quantity A may be written as $\Delta A = \vec{F}\cdot\vec{E}$. There are only a few physical examples of such a linear relationship between a polar vector and a scalar. The best known is the pyroelectric effect. The properties of $\vec{F}$ in different point group symmetries have been described by Voigt.[4] In our case the symmetry at the nuclear site should be taken. The relationship between the anisotropic hyperfine tensor and the electric field is described by a third order tensor. The phenomenology of this case has been discussed before.[1]

A quite general expression for the effect which is bilinear in the contact hyperfine interaction and the electric field can be written down by means of second order perturbation theory:

$$\Delta A_N = (8\pi/3) g g_N \beta\beta_N \sum_i \frac{(0|\delta(\vec{r}-\vec{r}_N)|i)(i|\mathcal{H}_E|0)}{W_0 - W_i} + \text{complex conj.} \qquad (1)$$

The electric field operator $\mathcal{H}_E = -\sum_k e_k E x_k$ is odd and $\delta(\vec{r} - \vec{r}_N)$ is even with respect to the nucleus as origin, $\vec{r}_N = 0$. A nonvanishing result is obtained only if the wave functions of both the ground state $|0\rangle$ and the excited state $|i\rangle$ contain some s character, and in addition are hybridized by some p-wave functions. A necessary condition is that the nucleus is not at a center of inversion symmetry.

The effects described above are observable, for example, in MnF_2. The F^{19} resonance has been thoroughly investigated in both the paramagnetic and antiferromagnetic regions.[5,6] The tetragonal crystal structure is well known and has the symmetry D_{4h}. All Mn^{++} ions are at a center of symmetry. There will be no linear effect of an electric field on the dimension of the unit cell nor on the magnetic properties of the Mn^{++} sublattices. The symmetry at the F^{19} nuclei at positions $\pm(u, u, 0)$, $\pm(u, -u, \frac{1}{2})$, is, however, orthorhombic, $mm2$ or C_{2v}. The polar vector $\vec{F}$ has one nonvanishing component. It has the same magnitude for each of the four F^- ions in the unit cell, but points in the four directions [110], [$\bar{1}$10], [1$\bar{1}$0], and [$\bar{1}\bar{1}$0].

Equation (1) is not suitable for explicit calculations, because the wave functions of the excited states are not known. The magnitude of the effect is determined, as in the case of quadrupole interaction, by the change in interionic distances and by the change in covalent character and s-p hybridization on application of an electric field.

The change in interionic distances gives a large effect in the mostly ionic crystal of MnF_2. Benedek and Kushida[6] have determined the variation of the contact interaction A with hydrostatic pressure. In their case the dimensions of the unit cell, a and c, are varied, whereas u was essentially constant. If an electric field is applied, u changes, but a and c are constant. The variation in u can be estimated from the contribution of the ionic displacements to the dielectric polarization,

$$\Delta r_{II} = \Delta u a\sqrt{2} = \left(\frac{\epsilon_\perp - n_\perp^2}{4\pi N e}\right) E. \qquad (2)$$

The ad hoc assumption has been made that the force constants on each F^- ion are isotropic in the (001) plane. $\epsilon_\perp$, the dielectric constant, and $n_\perp$, the index of refraction, are assumed to be equal to the values in CaF_2, $\epsilon = 6.8$ and $n = 1.44$. N is the number of F^- ions/cm^3; r_{II} is the variation in distance to the nearest Mn^{++} ion. The distance to the two other nearest neighbor Mn^{++} ions of type I varies by $\Delta r_I = \Delta r_{II} \sin\delta = 0.63 \Delta r_{II}$.

Take the Mn^{++} ion at (0, 0, 0) with spin down. Consider an electric field of 10^4 volts/cm applied along [110]. The F^{19} nucleus at $(u, u, 0)$ will move closer to the Mn^{++} with spin down and away from two Mn^{++} ions with spin up. The local magnetic fields and their variation due to displacement are listed in the first two columns of Table I, for complete spin alignment on the antiferromagnetic sublattices. The variations for the F^{19} nucleus at $(-u, -u, 0)$ have the opposite sign. The experimental results of Benedek and Kushida have been used to calculate $(\partial H/\partial u)$. It is not necessary to make theoretical assumptions about the nature of the bond at this stage. Either the exchange correlation in overlapping ionic orbitals[6] or an admixture of covalent orbitals[5,7] will give this variation of the contact interaction with interionic distance.

In covalent orbitals there is, however, another contribution given in the last column of Table I. The electric field will change the degree of covalency λ^2 and the degree of sp hybridization $s^2 = 1 - p^2$, at constant interatomic distance.[3] Although complete expressions are obtainable with the Ritz variational method, the following approximations will suffice for our present purpose:

$$\left(\frac{\partial s}{\partial E}\right)_u = \frac{-e\langle x_{sp}\rangle (1 - s^2)^{1/2}}{W_{2p} - W_{2s}} \times \tfrac{1}{3}(\epsilon_\perp + 2), \qquad (3)$$

Table I. Contributions to the magnetic field acting on the F^{19} nucleus at $(u, u, 0)$ in antiferromagnetic MnF_2 with complete spin alignment, and their variation in an electric field along [110]; $E = 10^4$ volts/cm.

	H_∞ (kilogauss)	$(\partial H_\infty/\partial u)(\partial u/\partial E)E$ (gauss)	$(\partial H_\infty/\partial E)_u E$ (gauss)
Dipolar	12.50	+0.425	0
Contact hyperfine	25.7	-13.6	-14
Anisotropic hyperfine	1.66	...	...

$$\frac{1}{\lambda}\left(\frac{\partial\lambda}{\partial E}\right)_u = \frac{e\gamma}{W_{\mathrm{Mn}} - W_{\mathrm{F}}} \times \tfrac{1}{3}(\epsilon_\perp + 2). \qquad (4)$$

The factor $E_{\mathrm{loc}}/E = \frac{1}{3}(\epsilon + 2) = 2.9$ relates the local field at the position of the bond to the applied field E. The Lorentz relationship has been assumed, although this, of course, is not strictly valid at a noncubic site. The energy difference between the $2s$ and $2p$ level of the fluorine atom is $W_{2p} - W_{2s} \sim 20$ ev; $e\langle x_{sp}\rangle$ is the dipole moment matrix element connecting these states, which may be calculated with Slater-type orbitals. $W_{\mathrm{Mn}} - W_{\mathrm{F}}$ is the energy necessary to transfer an electron from a F^- ion to the Mn^{++} ion in the lattice, and is rather arbitrarily taken as 5 ev. The contact hyperfine interaction is proportional to $\sum \lambda_j^2 s_j^2$, where the summation is over the three nearest Mn neighbors. Note that the degree of covalency and s character increases if the F atom moves toward the Mn atom. The total relative variation of the hyperfine interaction at constant u is approximately

$$(\Delta H/H)_u = [2(\Delta\lambda/\lambda) + 2\Delta s/s](1 + 2\sin\delta). \qquad (5)$$

Take $s = \frac{1}{2}$ corresponding to 25% s character, while $\lambda^2 = 0.02$. It turns out that the variation in λ contributes an order of magnitude more than the variation in s. Combination of Eqs. (3)-(5) gives the value -14 gauss in the last column.

One finds from Table I that the total relative variation of the F^{19} resonance frequency in antiferromagnetic MnF_2 is $|\Delta\nu_E|/\nu_0 = 0.67 \times 10^{-4}$ for $E = 10^4$ volts/cm along [110]. This corresponds to $\Delta\nu_E = 108$ kc/sec since $\nu_0 = 160$ Mc/sec at 4.2°K. Since the linewidth is only 50 kc/sec, the effect should be readily observable. Experiments are at present under way. They should give valuable information about the covalent contribution and test the correctness of the theoretical assumptions.

The p-type or anisotropic hyperfine interaction depends sensitively not only on the σ orbital considered above, but also on the π and π' orbitals.[7] A calculation of its dependence on electric field will be postponed until a more complete account can be given. The contribution to the F^{19} resonance frequency is estimated to be at least one order of magnitude smaller than the other entries in Table I.

The dipolar and anisotropic hyperfine interaction also produce a magnetic field H_x in the [110] direction at right angles to the z axis of quantization of the F^{19} spin. Consider the dipolar term,

$$-g_N\beta_N H_x I_x = -\tfrac{3}{2}\sin\delta\cos\delta \times r^{-3} g\beta g_N\beta_N \langle S_z\rangle (I^+ + I^-). \qquad (6)$$

One finds $\Delta H_x = -0.6$ gauss if an electric field of 10^4 volts/cm is applied at 4.2°K. If the electric field is alternating at the resonant frequency of the F^{19} spins, it will induce nuclear spin transitions. At 4.2°K the F^{19} resonance can be saturated electrically. This situation is rather unusual, in that a spin $I = \frac{1}{2}$ is "tickled" by an applied electric field.

Finally it is pointed out that the isomer shift,[8] which is also proportional to $|\psi^2(0)|$, will be a function of the electric field, if the nucleus is at a suitable lattice site. Since the relative variation in $|\psi^2(0)|$ of the valence electrons is about $1{:}10^3$ for 10^5 volts/cm, the effect will be near the limit of detectability for the Mössbauer effect.

---

[1]J. Armstrong, N. Bloembergen, and D. Gill, Phys. Rev. Letters 7, 11 (1961).

[2]T. Kushida and K. Saiki, Phys. Rev. Letters 7, 9 (1961).

[3]J. Armstrong, N. Bloembergen, and D. Gill, J. Chem. Phys. (to be published); N. Bloembergen, J. Chem. Phys. (to be published).

[4]W. Voigt, Lehrbuch der Kristallphysik (B. G. Teubner, Leipzig, 1910).

[5]R. G. Shulman and V. Jaccarino, Phys. Rev. 108, 1219 (1957).

[6]G. B. Benedek and T. Kushida, Phys. Rev. 118, 46 (1960).

[7]M. Tinkham, Proc. Roy. Soc. (London) A236, 535 and 549 (1956).

[8]L. R. Walker, G. K. Wertheim, and V. Jaccarino, Phys. Rev. Letters 6, 98 (1961).

IMAGE OF THE FERMI SURFACE IN THE LATTICE VIBRATIONS OF LEAD

B. N. Brockhouse, K. R. Rao,* and A. D. B. Woods
Neutron Physics Branch, Atomic Energy of Canada Limited, Chalk River, Ontario, Canada
(Received June 26, 1961)

On theoretical grounds Kohn[1] has proposed that there should exist positions in reciprocal space at which the slopes of the dispersion curves of the lattice vibrations in metals become infinite. The positions are related to the Fermi surface of the electrons, and the infinite slope to the sharpness of the Fermi surface. These Kohn anomalies have not previously been observed experimentally for certain, and recent calculations[2] suggest that they may be quite small, at least for some materials. We believe that we have observed the anomalies in a single cyrstal of lead.

Previous experiments[3] on lead at this laboratory yielded dispersion curves which could be interpreted on the Born-von Kármán theory of lattice dynamics only if it were assumed that there exist long-range forces between ions in the crystal, the forces often varying in sign. These results were consistent with the existence of Kohn anomalies, but direct evidence was weak.

The new experiments were carried out using the triple-axis crystal spectrometer in such a way that, for each energy distribution, the momentum transfer, $\hbar\vec{Q}=\hbar(\vec{k}_0-\vec{k}')$, remained fixed.[4] The centers of the neutron groups observed give the frequencies ν of the lattice vibrations (of wave vector $\vec{Q}$ in the extended zone scheme) through the relation $h\nu=E_0-E'$. In the expressions $\vec{k}_0$ and $\vec{k}'$ and E_0 and E' are the incoming and outgoing neutron wave vectors and energies, respectively.

Figure 1(a) shows a series of neutron groups obtained as the terminus of $\vec{Q}$ moves along the line $\vec{Q}=(2\pi/a)[\zeta,\zeta,\zeta]$ between the reciprocal lattice points (1, 1, 1) and (2, 2, 2) in steps of 0.025 in ζ. (a is the lattice constant.) The neutron groups observed correspond to longitudinal phonons whose reduced wave vector $\vec{q}$ is in the [111] direction of the Brillouin zone. The centers of the groups are shown plotted in Fig. 1(b) as a function of $(a/2\pi)\vec{Q}$. Near the zone boundary a sharp anomaly occurs on both sides of the zone boundary, as it should, and three independent series of measurements at different energies gave almost identical results.

For a spherical Fermi surface the positions of the anomalies are given[1] by the equation

$$2K_F=|2\pi\vec{\tau}+\vec{q}|,$$

where $\vec{\tau}$ is a vector of the reciprocal lattice and K_F is the radius of the Fermi surface. In Fig. 2 the $(1\bar{1}0)$ plane of reciprocal space is shown, each reciprocal lattice point, $a\vec{\tau}$, surrounded by its zone. A spherical Fermi surface containing four

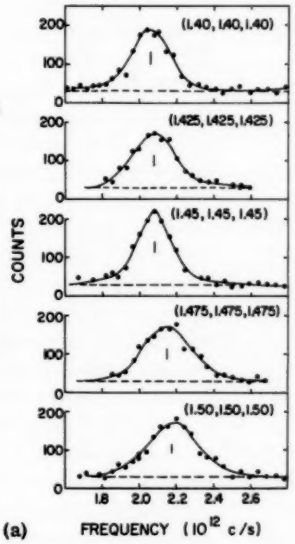

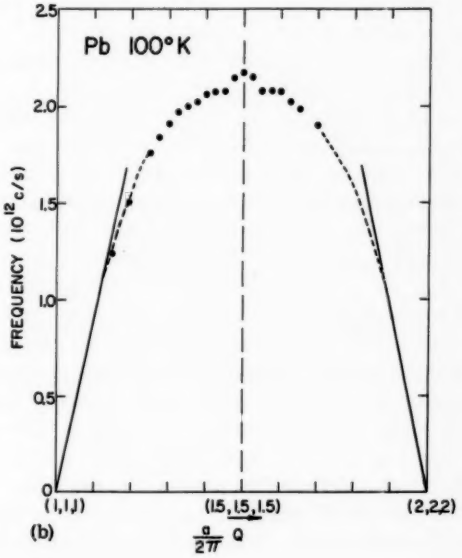

FIG. 1. (a) A series of neutron groups (actual counts) obtained for values of $\vec{Q}$ along the line $\vec{Q}=(2\pi/a)[\zeta,\zeta,\zeta]$ from $\zeta=1.4$ to $\zeta=1.5$, for $E'=0.01228$ ev. The background is indicated by the dashed line. (b) The frequency corresponding to neutron groups observed along the line $\vec{Q}=(2\pi/a)\times[\zeta,\zeta,\zeta]$. The dashed line corresponds to the previously measured dispersion curve for the longitudinal [111] branch. The solid lines have the slope of the velocity of sound as calculated from the elastic constants.

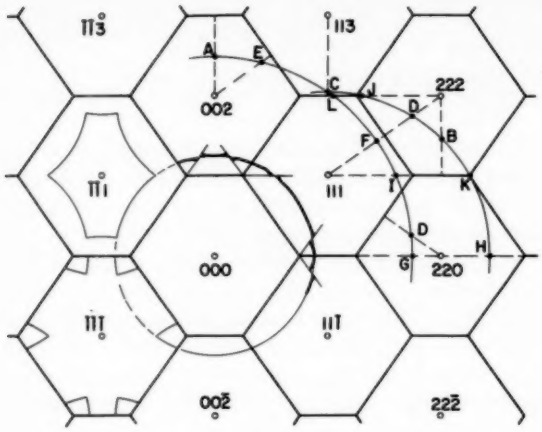

FIG. 2 The (1$\bar{1}$0) plane of the reciprocal lattice of (face-centered cubic) lead, each point surrounded by its zone. A spherical Fermi surface containing four free electrons (extended zone scheme) intersects the plane as shown by the circle about the point (0,0,0). In the reduced zone scheme this spherical surface gives rise to the surface shown about ($\bar{1}$,$\bar{1}$,1) in the second zone, and to the surfaces shown about ($\bar{1}$,$\bar{1}$,$\bar{1}$) in the third zone. Possible effects of gap formation on the extended zone surface are indicated by bold lines. The Kohn construction for free electrons is shown by the circular arcs *AECLFIDG* and *CJDBKH*. The points *A*, *B*···*L* indicate positions of Kohn anomalies for free electrons in the symmetric directions [100], [110], and [111], shown by dashed lines.

electrons[5,6] is drawn around the point $a\vec{\tau} = (0, 0, 0)$. In the reduced zone scheme this Fermi surface gives a full first zone, a second zone with a pocket of holes as shown around the point ($\bar{1}$, $\bar{1}$, 1), and a complicated structure in the third zone shown in cross section around the point ($\bar{1}$, $\bar{1}$, $\bar{1}$). The locus of the Kohn anomalies connected with the point (0, 0, 0) is shown as the circular arc *AECLFIDG*. Other types of anomalies also occur, as indicated by the arc *CJDBKH* which is connected with the point (2, 0, 0) [a point not in the (1, $\bar{1}$, 0) plane]. The positions designated by the letters *A*, *B*, ···, *L* are those for which anomalies in the symmetric [100], [110], and [111] directions of the reduced zone occur for a spherical Fermi surface. Some of the anomalies have a multiplicity greater than unity, because they can be produced from several reciprocal lattice vectors (e.g., *E* with multiplicity 3, *C* with 4, *H* with 2, etc.). Some of the anomalies can occur only in longitudinal modes (e.g., *A*, *F*, *G*); these have unit multiplicity. The signs of the anomalies (i.e., $\operatorname{grad}_{\vec{q}}\nu = +\infty$ or $-\infty$) can be assigned by the plausible rule that the frequency increases anomalously when $\vec{q}$ passes from the interior to the exterior of the Kohn sphere since the electron gas then "stiffens." Thus *A*, *E*, *F*, and *I* have positive signs, while *C*, *D*, and *G* have negative signs.

The spherical Fermi surface applies to ideally free electrons. In fact energy gaps will be produced at Bragg reflection planes, as illustrated by the modifications to the spherical Fermi surface shown as bold lines in Fig. 2. These gaps round off the Fermi surfaces in the reduced zone, and render the Kohn construction[1] more complicated. In particular, only points *A*, *F*, *G*, and possibly *I*, are certain to be unchanged in a qualitative sense by the passage to the real Fermi surface.

It will be observed that point *F*, expected to occur only in the longitudinal mode, corresponds very closely to the anomaly in Fig. 1(b). However, this assignment is ambiguous because of possible interference with point *E*.

In Fig. 3 the longitudinal branch for the [110] direction is shown. These measurements were made along three separate lines through reciprocal space; from (2, 2, 0) to (1, 1, 0), from (2, 2, 0) to (3, 3, 0), and from (1, 1, 1) to (2, 2, 1). Two different monochromator planes were used from (2, 2, 0) to (1, 1, 0). An anomaly, which can be identified with point *G*, appears at $aq/2\pi \simeq 0.40$. The position of the anomaly yields the result that the radius of the Fermi surface in the [110] direction (extended zone scheme) is about $1.21(2\pi/a)$, instead of the value $1.24(2\pi/a)$ holding for free electrons. Thus the width of the arms in the third zone (reduced zone scheme) is smaller by about 15% than for free electrons, in qualitative agreement with deductions by Gold[5] from his measurements on the de Haas–van Alphen effect. [Note added: From inspection of Fig. 3, Kohn and Woll (private communication) would place the anomaly at ~0.47, and thus make the width about one third smaller than for free electrons.]

Many other features of the unusual dispersion curves of lead[3] may be interpreted in terms of the Kohn effect. Of particular interest is the spectacular drop in frequency found for the longitudinal branch in the [100] direction near the zone boundary, which may be connected with anomaly *C*. This anomaly has fourfold multiplicity and therefore should be exceptionally strong. However, details are not clear since this point is strongly influenced by gap formation at the (002) Bragg plane, as indicated in Fig. 2.

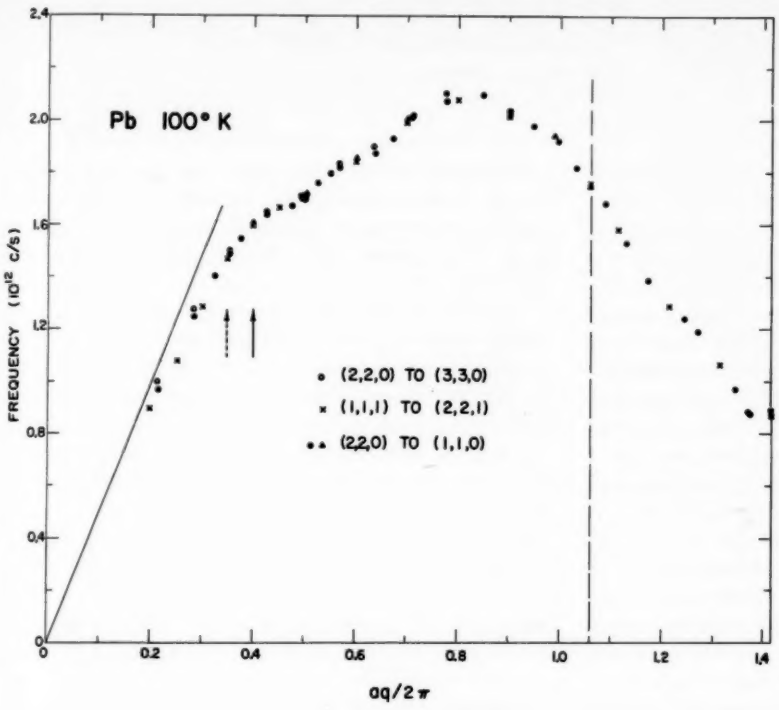

FIG. 3. The longitudinal branch in the [110] direction of the reduced zone. The branch is continued beyond the zone boundary to the point (1,1,0). The continuation, lying on the square face of the Brillouin zone, has the same symmetry as the [110] direction within the zone. The anomaly assigned as G is indicated by the solid vertical arrow at $qa/2\pi \simeq 0.40$. For free electrons it would appear at 0.35 as indicated by the dashed arrow. Other possible anomalies can also be seen. Measurements in a single series are thought to have relative errors about the size of the points. The scatter in points belonging to different series may be indicative of the absolute errors.

As mentioned earlier, recent calculations[2] have indicated that the anomalies should be quite small. The strength of the effect in lead is probably connected with the strong phonon-electron interaction in this material, as indicated for example by the comparatively high superconducting transition temperature. This is supported by the fact that the Kohn effect has not been detected in similar measurements on a single crystal of sodium.[7]

The anomalies are, of course, smeared out by resolution in $\vec{q}$ space. (Indeed, Fermi surfaces may be more easily delineated by means of x-ray intensity measurements than by neutron measurements, because of the better resolution in $\vec{q}$ space available with x rays.) However, even under good resolution the anomalies will appear to be smeared because of the logarithmic character of the infinity in the slope, which makes exceedingly small the range in ν over which $|\mathrm{grad}_{\vec{q}}\,\nu|$ is large.

Dr. G. Caglioti participated in an earlier, inconclusive, attempt to detect the effect in lead. E. A. Glaser gave valuable technical assistance.

---

*Visiting scientist from Atomic Energy Establishment, Trombay, Bombay, India.

[1]W. Kohn, Phys. Rev. Letters 2, 393 (1959).

[2]E. J. Woll and S. J. Nettel, Bull. Am. Phys. Soc. 6, 144 (1961). Also S. H. Vosko (private communication).

[3]B. N. Brockhouse, T. Arase, G. Caglioti, M. Sakamoto, R. N. Sinclair, and A. D. B. Woods, International Atomic Energy Agency Symposium on Inelastic Scattering of Neutrons in Solids and Liquids, Vienna, October, 1960 [issued as Chalk River Laboratory Report CRNP-946, AECL No. 1074 (unpublished)].

[4]B. N. Brockhouse, see reference 3 [issued as Chalk River Laboratory Report CRNP-947, AECL No. 1183 (unpublished)]; also Bull. Am. Phys. Soc. 5, 462 (1960).

[5]A. V. Gold, Trans. Roy. Soc. (London) A251, 85 (1958).

[6]W. A. Harrison, Phys. Rev. 118, 1190 (1960).

[7]A. D. B. Woods, B. N. Brockhouse, R. H. March, and R. Bowers, Bull. Am. Phys. Soc. 6, 261 (1961).

DISSOCIATION OF H_2^+ IONS BY A MAGNETIC FIELD*

Selig Kaplan, George A. Paulikas, and Robert V. Pyle
Lawrence Radiation Laboratory, University of California, Berkeley, California
(Received July 10, 1961)

The dissociation of molecular ions by an externally applied electric field, $\vec{E}$, or an equivalent electric field, $\vec{E}' = \vec{v} \times \vec{B}$, due to motion through a magnetic field has been calculated by Hiskes.[1] Qualitatively, it is predicted that the external fields warp the nuclear potential in such a way that the higher vibrational states become unstable and dissociation results. This effect has been observed recently by Riviere and Sweetman,[2] who dissociated H_2^+ and H_3^+ ions of approximately 2-Mev energy with electric fields of up to 5×10^5 v/cm. The measurements presented here demonstrate the breakup of molecular hydrogen ions of 10 Mev per nucleon by static magnetic fields.

The experimental arrangement is shown in Fig. 1. Ions produced in a P.I.G. discharge were accelerated in the Berkeley heavy-ion linear accelerator (Hilac). H_2^+ and H_3^+ ions were continuously accelerated to full energy, and, alternatively, full-energy H_2^+ ions were obtained by partially stripping 3-Mev H_3^+ ions in a jet of Hg vapor and then accelerating the resulting H_2^+ ions to 20 Mev. The reason for producing H_2^+ by the latter technique is that such ions might be left in more highly excited states than those which came directly from the ion source, as demonstrated by Riviere and Sweetman. The ions emerged from the Hilac accompanied by other particles formed by breakup on the residual gas in the vacuum system. The beam was collimated to $\frac{3}{16} \times \frac{3}{16}$ in., and the various particles were then separated by bending the useful beam by 15 deg in a dc magnetic field. No further collimation was required, thus eliminating background from breakup at slit edges.

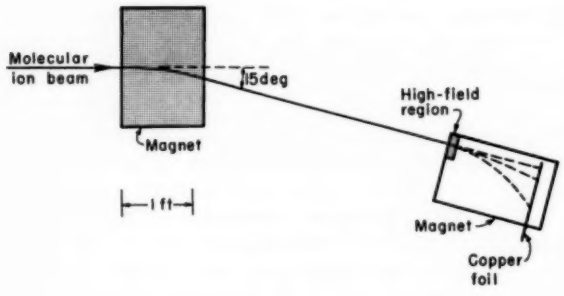

FIG. 1. Experimental arrangement.

The dissociation and analysis were obtained in a dc magnet with a 4-in. gap. The gap in the first 1.5 in. of the magnet could be reduced to 1 in., thereby producing a maximum magnet field of about 19 kilogauss. The beam required about 10^{-9} second to traverse this region.

The results reported here were obtained by activating 0.010-in. thick Cu foils, placed in the analyzing magnet perpendicular to the direction of the incident beam. The foil holder was built to serve as a Faraday cup, and was used in the beam-monitoring system. The spatial distribution and the relative intensities of the beam particles (i.e., H^0, H_1^+, H_2^+, etc.) were determined by counting the Zn^{63} activity ($T_{1/2} = 38$ min) produced in the foil.

Briefly, the scanning was done as follows: The bombarded Cu foil was wrapped around a rotating wheel whose instantaneous position was synchronized with the voltage of a linear ramp. A NaI crystal viewed the wheel through a slit in a W and Pb shield. Whenever a 0.51-Mev annihilation γ ray from Zn^{63} decay was detected in the crystal, a pulse of height equal to the ramp voltage was generated. These pulses were put into a Penco 100-channel pulse-height analyzer, and a presentation of count rate vs position on the foil was obtained.

The dissociation caused by the residual gas in the vacuum system at our base pressure of about 6×10^{-6} mm Hg was determined by raising the pressure in several steps by adding N_2, measuring the dissociation, and extrapolating to the base pressure.

The H_2^+ ions obtained by stripping H_3^+ were partially dissociated by the magnetic field, with a rapid rise at about 12 kilogauss. This magnetic field corresponds to approximately 5×10^5 v/cm (Fig. 2). Our result is consistent with the dissociation of the $v = 17$ vibrational state as calculated by Hiskes for nonrotating molecules. The vertical bands marked 10^{-8} sec and 10^{-14} sec indicate the calculated fields necessary for barrier penetration in these times, with the widths of the bands corresponding to the uncertainties. The field in the 15-deg bending magnet was sufficiently high to have already dissociated the $v = 18$ vibrational state if it were populated. Conversely, the maximum stripping field was somewhat too low to affect the $v = 16$ state.

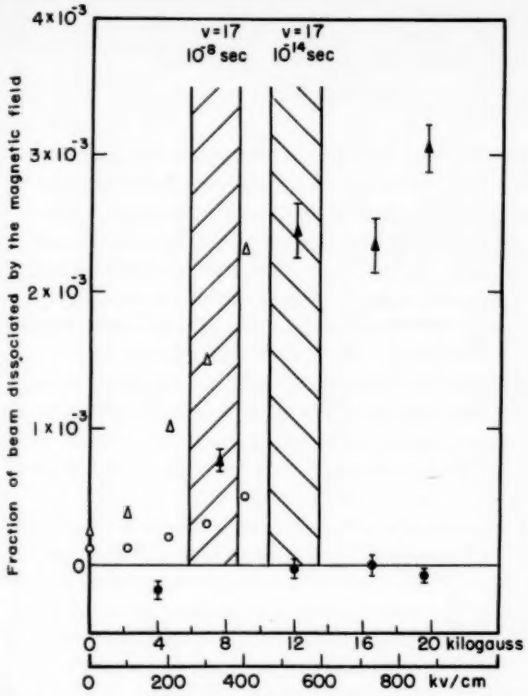

FIG. 2. Fraction of the beam dissociated by magnetic fields (present experiment) and electric fields (Riviere and Sweetman). ▲, magnetic, H_2^+ from H_3^+; ●, magnetic, H_2^+ direct; △, electric, H_2^+ from H_3^+; ○, electric, H_2^+ direct. A background-gas breakup corresponding to a fractional dissociation of $(0.26 \pm 0.04) \times 10^{-3}$ has been subtracted from the magnetic dissociation data. The standard deviations shown include counting statistics, an estimated uncertainty of 15% in the extrapolated dissociation by the residual gas in the vacuum system, and an uncertainty of 5% in the calibrations of foil activity vs ion current.

No indication of magnetic field dissociation was obtained for the directly accelerated H_2^+ and H_3^+ ions. We have no theoretical information concerning the H_3^+ ion. The absence of dissociation of directly accelerated H_2^+ ions is assumed to be due to the method of formation and to possible de-excitation in the ion source.

With more suitable choices of the kind of ion, energy, and magnetic field strength, dissociation by a magnetic field might provide a mechanism for trapping ions in a highly evacuated controlled thermonuclear device, and provide a diagnostic tool for the study of molecular ion formation and excitation. We are extending this investigation to other molecular ions and to neutral atoms in similar and higher magnetic fields.

We wish to express our appreciation to Dr. C. M. Van Atta for supporting and encouraging this research, J. Warren Stearns and Henry F. Rugge for helping with the measurements, Dr. Edward L. Hubbard, Duane A. Spence, and other members of the Hilac staff for their assistance, John R. Meneghetti for much of the mechanical construction, and Dr. John R. Hiskes for many interesting and useful theoretical discussions. One of the authors (S. K.) would like to thank Professor Burton J. Moyer for the support and interest that enabled him to participate in this work.

---

*Work done under the auspices of the U. S. Atomic Energy Commission.

[1]J. R. Hiskes, Phys. Rev. 122, 1207 (1961).

[2]A. C. Riviere and D. R. Sweetman, Phys. Rev. Letters 5, 560 (1960).

ROTATIONAL BANDS IN Ne^{20}

A. E. Litherland, J. A. Kuehner, H. E. Gove, M. A. Clark, and E. Almqvist
Atomic Energy of Canada Limited, Chalk River, Ontario, Canada
(Received June 30, 1961)

In recent years evidence has been obtained[1,2] which strongly suggests that the low-lying levels of Mg^{24}, Mg^{25}, and Al^{25} can be arranged into rotation-like bands. In this Letter we discuss new evidence which suggests that the low-lying levels of Ne^{20} can also be arranged into overlapping rotational bands. A separation of the level spectrum of Ne^{20} into rotational bands is shown in Fig. 1. Ne^{20} is of great interest in this respect because it is close enough to the closed shell at O^{16} for detailed shell-model calculations to be feasible.[3]

Last year Broude and Gove[2,4] showed that the spins of the 4.25- and 4.97-Mev levels in Ne^{20} were 4 and 2 and that the quadrupole to dipole amplitude ratio for the cascade transition from the 4.97- to the 1.63-Mev level was +0.08. These results have been confirmed recently and the parities of the levels measured.[5-7] The parity of the 4.97-Mev level was found unexpectedly to be negative and the astrophysical implications of this measurement have been discussed recently.[7] Measurements on the lifetimes of the levels in Ne^{20} using the Doppler shift attenuation method[8,9] and Coulomb excitation[10] have indicated that the electric quadrupole transitions from the 1.63-Mev level and the 4.25-Mev level were enhanced some twenty times over the single-particle estimate. The spins, parities, and lifetimes of the first three levels of Ne^{20} suggest that they form the first three members of a perturbed rotational band. Preliminary evidence for a level in Ne^{20} at about 7.6 Mev has been obtained recently in a study of gamma-gamma coincidences[11] and a magnetic spectrometer analysis[12] of the alpha particles from the reaction $C^{12}(C^{12},\alpha)Ne^{20}$. This level has some of the properties required for a 6+ level but is shown dashed in Fig. 1 because of the preliminary nature of the evidence.

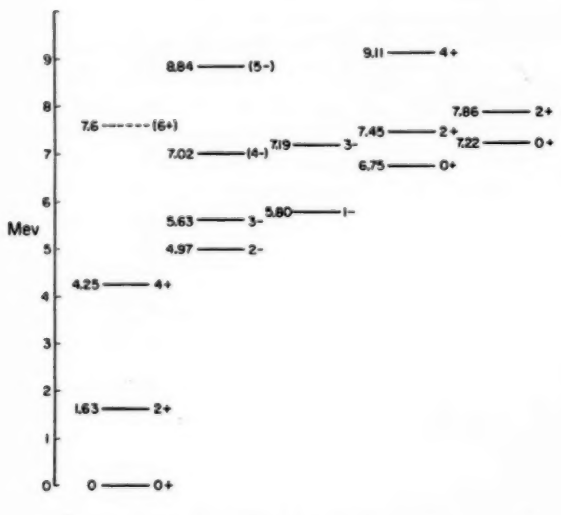

FIG. 1. A separation of the level spectrum of Ne^{20} into rotational bands. A level in Ne^{20} above about 4.75 Mev can break up into O^{16} and an alpha particle if its parity is $(-1)^J$.

Measurements[13] have been made which showed that the spins and parities of the 5.63-Mev level and of a level reported recently by Adams et al.[14] at 5.80 Mev are 3- and 1-, respectively. These assignments together with the measured values[15] of Γ_γ/Γ of 0.07(±0.01) and 0.003 (±0.003) show that both these levels, like the 2- level at 4.97 Mev, have strongly inhibited $E1$ de-excitation widths. Bearing in mind the rotation-like band based on the ground state of Ne^{20}, it was conjectured that the 2-, 4.97-Mev level, the 3-, 5.63-Mev level, and the (5-), 8.84-Mev level[16] formed a negative-parity band. A 4- level would then be expected at an excitation of about 7 Mev. The enhancement of $E2$ transitions within the ground-state rotational band and the strong inhibition of the $E1$ transitions from the 4.97-, the 5.63-, and 5.80-Mev levels[10,15] suggested that the 4- level, if it exists and if it is indeed a member of the postulated rotational band, should decay by $E2$ transitions to the 2-, 4.97-Mev and the 3-, 5.63-Mev levels in strong competition with a possible $E1$ decay to the 4+, 4.25-Mev level.

A new level in Ne^{20} at 7.02 Mev, exhibiting several of the expected properties, has now been located using the $C^{12}(C^{12},\alpha\gamma)Ne^{20}$ reaction. The new level shows gamma-ray transitions to the 2-, 4.97-Mev level and the 3-, 5.63-Mev level with relative intensity approximately 2:1. It is interesting to note that if these gamma-ray transitions are pure electric quadrupole the collective model predicts[17] a relative intensity of 3:1. No other cascade gamma rays with intensities greater than 15% of that for the transition to the 4.97-Mev level have been observed. Alpha-gamma angular correlations are consistent with spin and parity of

4- but do not conclusively prove this assignment. Recent measurements[12] of alpha-particle spectra using a magnetic spectrometer at 0°, 10°, and 50° to the beam show that the 7.02-Mev state very probably has parity $(-1)^{J+1}$.

In Fig. 2 the energy levels of Ne^{20} are plotted as a function of $J(J+1)$. In this plot one can see deviations from the simple rotational expression, $E(J)=(\hbar^2/2\mathcal{I})J(J+1)$. The lines connecting states of each rotational band are expected to be approximately parallel and this appears to be the case. The average slope of the lines, which is equal to $\hbar^2/2\mathcal{I}$, is approximately 150 kev. This may be compared with a slope of about 135 kev expected for the rotations of a rigid spheroid of distortion parameter[1] $\delta \sim 0.3$. The dashed lines shown in Fig. 2 are possible extensions of the rotational bands.

The absence of a 1- level below the 2-, 4.97-Mev level indicates that the band based on that level can be assigned a K-quantum number of 2. Possible levels of spin and parity 2- and 4-, which might be members of the band based on the 1-, 5.80-Mev level, have not yet been observed and the present evidence suggests that they do not exist. This point is of interest because the 1-, 5.80-Mev level and the 3-, 7.19-Mev levels may then be the first two members of a band with $K=0$. If negative-parity bands with $K=0$ and $K=2$ can be established conclusively, then it is possible that these bands may be explained as rotations of the Ne^{20} nucleus which is undergoing surface octupole vibrations.[18] The alternative explanation that the negative-parity bands are based upon states of particle excitation must also be considered. According to the Nilsson model,[19] the lowest of these is expected to be a configuration in which one particle is removed from the [101] level and put into the [211] level. Such particle configurations would give rise to two bands of $K=1-$, $J=1, 2, 3$, etc., and $K=2-$, $J=2, 3, 4$, etc. Calculations[20] indicate that these bands would not occur as low as 5 Mev in Ne^{20} and the absence of the $J=2-$ level at ~6.3 Mev argues against a $K=1$ assignment to the band based on the $J=1-$ level at 5.8 Mev.

Clearly more experimental evidence is required on the existence of other band members and their properties before a complete account of Ne^{20} is possible. However, the collective model gives a good account of the properties of the low-lying levels of Ne^{20} which are known at present.

We would like to acknowledge the stimulating interest shown in this work by Dr. L. G. Elliott.

[1]A. E. Litherland, H. McManus, E. B. Paul, D. A. Bromley, and H. E. Gove, Can. J. Phys. 36, 378 (1957).

[2]H. E. Gove, Proceedings of the International Con-

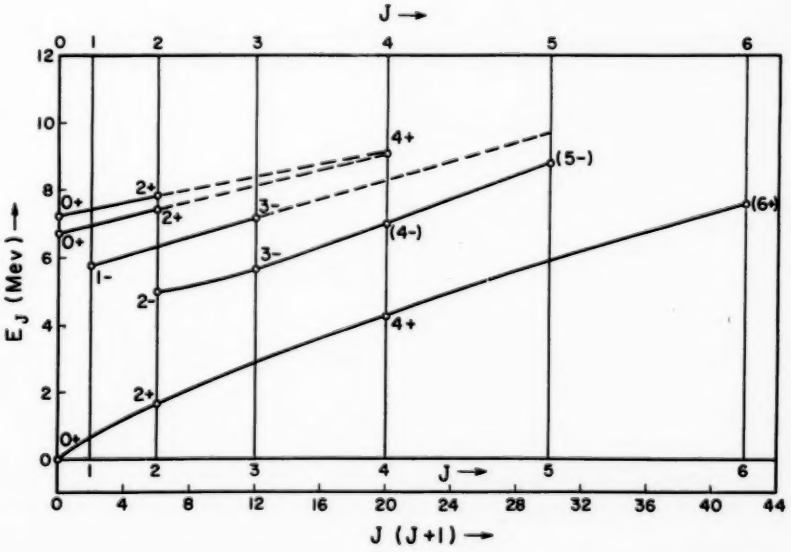

FIG. 2. The energies of the levels in Ne^{20} are plotted against $J(J+1)$, where J is the total angular momentum of the level. Solid lines join the levels that are suspected to form rotational bands.

ference on Nuclear Structure, edited by D. A. Bromley and E. Vogt (University of Toronto Press, Toronto, 1960), p. 438 ff.

[3]J. P. Elliot, Proc. Roy. Soc. (London) A245, 128 (1958).

[4]C. Broude and H. E. Gove, Bull. Am. Phys. Soc. 6, 37 (1961).

[5]H. E. Gove, A. E. Litherland, and M. A. Clark (to be published).

[6]E. Almqvist, D. A. Bromley, J. A. Kuehner, and B. Whalen (to be published).

[7]H. E. Gove, A. E. Litherland, and M. A. Clark (to be published).

[8]S. Devons, G. Manning, and J. H. Towle, Proc. Phys. Soc. (London) A69, 173 (1956).

[9]M. A. Clark, H. E. Gove, and A. E. Litherland, Bull. Am. Phys. Soc. 6, 249 (1961), and to be published.

[10]I. Kh. Lemberg, Proceedings of the Second Conference on Reactions Between Complex Nuclei, edited by A. Zucker, E. C. Halbert, and F. T. Howard (John Wiley & Sons, New York, 1960), p. 112.

[11]A. E. Litherland, M. A. Clark, and H. E. Gove (to be published).

[12]E. Almqvist and J. A. Kuehner (to be published).

[13]J. A. Kuehner (to be published).

[14]H. S. Adams, J. D. Fox, N. P. Heydenburg, and G. M. Temmer, Bull. Am. Phys. Soc. 6, 250 (1961), and private communication.

[15]J. A. Kuehner and E. Almqvist (to be published).

[16]L. C. McDermott, K. W. Jones, H. Smotrich, and R. E. Beneson, Phys. Rev. 118, 175 (1960).

[17]G. Alaga, K. Alder, A. Bohr, and B. Mottelson, Kgl. Danske Videnskab. Selskab, Mat.-fys. Medd. 29, No. 9 (1955).

[18]P. O. Lipas and J. P. Davidson, Bull. Am. Phys. Soc. 6, 232 (1961).

[19]B. R. Mottelson and S. G. Nilsson, Kgl. Danske Videnskab. Selskab, Mat.-fys. Skrifter 1, No. 8 (1959).

[20]T. D. Newton (private communication).

PARTICLE PRODUCTION BY 10-30 Bev PROTONS INCIDENT ON Al AND Be†

W. F. Baker, R. L. Cool, E. W. Jenkins, T. F. Kycia, S. J. Lindenbaum, W. A. Love, D. Lüers,*
J. A. Niederer, S. Ozaki, A. L. Read, J. J. Russell, and L. C. L. Yuan
Brookhaven National Laboratory, Upton, New York
(Received June 21, 1961; revised manuscript received July 12, 1961)

High-energy secondary particles produced by the nuclear interactions of 10-30 Bev protons have been investigated at the Brookhaven alternating gradient synchrotron (AGS).[1] This experiment was carried out with aluminum and beryllium internal targets (according to availability) at production angles[2] of $4\frac{3}{4}°$, 9°, 13°, and 20°. The momentum of the particles in a beam was selected by magnetic deflection and the velocities determined with focusing, gas Čerenkov counters.[3] The momentum acceptance and angular divergence of the beams were fixed by scintillation counter telescopes. Typical values of these parameters were $\Delta p/p \simeq \pm 2\%$ and $\Delta\Omega \simeq 2\times10^{-7}$ steradian. The ratio of quadruple coincidences ($S_1S_2S_3C$) to triple coincidences ($S_1S_2S_3$) corrected when necessary for Čerenkov counter inefficiency gave the relative abundance of the particle of selected mass in a beam.

Most of the data were taken with the machine operated at 29.5 ± 0.5 Bev with an average intensity of ~4×10^{10} protons per pulse accelerated each 2.4 seconds. Measurements were also made at AGS energies of 25, 20, and 10 Bev, at which energies the machine can be operated at 2.0-, 1.6-, and 0.8-second repetition periods, respectively.

Figure 1 shows the momentum distributions of protons, π^+ and π^- mesons, corrected for π decay between the target and the final scintillator in order to represent the pion-production rates at the target. A rough correction has been made for the number of decay muons counted as pions. This correction was less than 5% of the measured pion intensity for beams of momentum >4 Bev/c. The muon contamination increased rapidly with decreasing momentum below 4 Bev/c; at 2.5 Bev/c the contamination was ~12% and at 1.25 Bev/c it

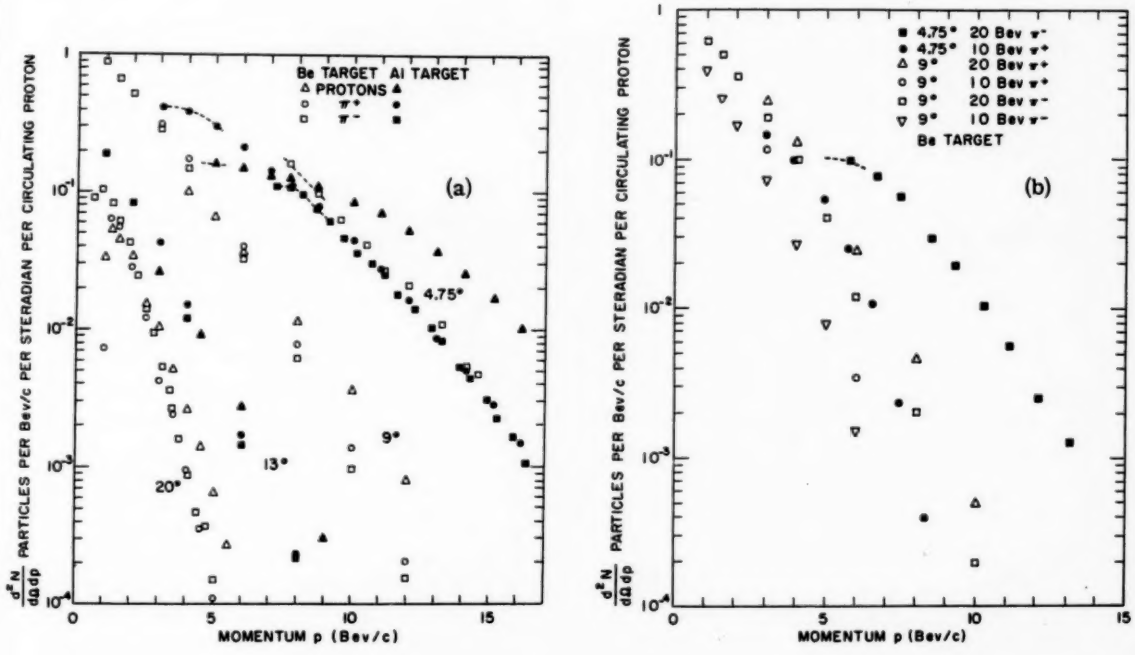

FIG. 1. The momentum spectra, (a) of $\pi^\pm$ mesons and protons for 30-Bev incident proton energy, and (b) of $\pi^\pm$ mesons for 10- and 20-Bev incident proton energies. The ordinate is the number of particles per steradian per Bev/c per circulating proton. The dashed portions of the $4\frac{3}{4}°$ spectra indicate the regions where the correction due to fringing field effects exceeds 15% of the measured value of $d^2N/dpd\Omega$.

was ~40%. The curves are normalized to the number of circulating protons in the AGS which has been calibrated by electrical methods to an accuracy of about 25%.[4] The effective target thickness for nuclear interactions was measured by radiochemical methods for both Al and Be targets.[5] The efficiencies of the targets have been estimated by Courant.[6] For Al the effective target thickness was 37 ± 7 g/cm^2, and for Be it was 21 ± 3 g/cm^2, corresponding to an efficiency for each target of ~50%. Thus, $2 \times d^2N/dp d\Omega$ approximately represents the number of particles produced per inelastic interaction with the target nucleus per steradian per Bev/c. Fluctuations in target efficiency may have been as much as ±10%.

Of the four beams measured, the magnetic field of the AGS strongly influences only the trajectory of the nominal $4\frac{3}{4}°$ beam. Thus in this beam the actual production angle varies from $3\frac{3}{4}°$ for negative particles of momentum 6 Bev/c to $5\frac{1}{2}°$ for positive particles of momentum 2 Bev/c; the production angle is 4.7° for very high momentum (i.e., ~20 Bev/c) particles of either sign of charge.[7] The fringing field of the AGS and the beam collimator combine to reduce the effective solid angle seen by the counter telescope. Corrections for these effects have been applied to the measured data; the dashed portions of the $4\frac{3}{4}°$ curves indicate the regions where these corrections exceeded 15%. Figures 2 and 3 and Table I show the ratios of the intensities K^+/π^+, K^-/π^-, and $\bar{p}/\pi^-$, measured in each beam at various momenta. The ratios measured experimentally have been corrected for K and π decay between the target and the final scin-

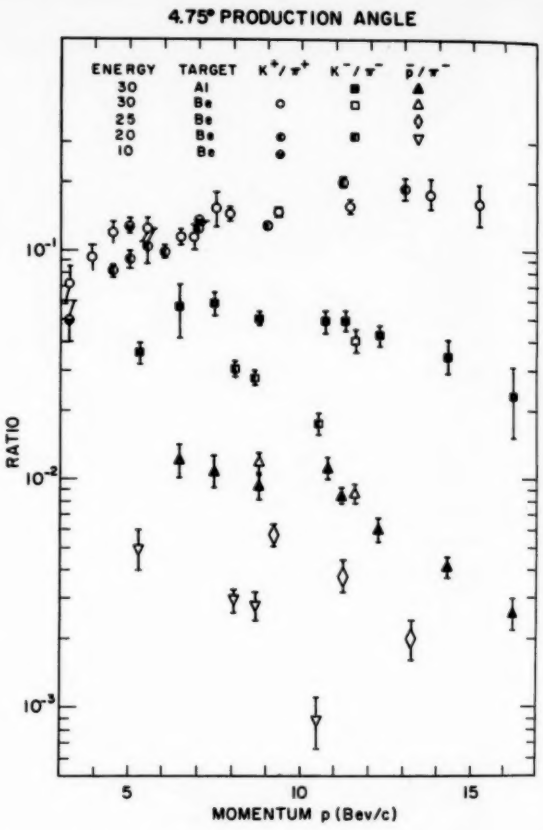

FIG. 2. The production ratios at the target of K^+/π^+, K^-/π^-, and $\bar{p}/\pi^-$ at various momenta, at $4\frac{3}{4}°$ production angle. The ratios have been corrected for K and π decay between the target and the final scintillator and for muon contamination.

Table I. The production ratios at the target of K^+/π^+, K^-/π^-, and $\bar{p}/\pi^-$ at various momenta for production angles of 13° and 20°. The AGS internal energy = 30 Bev. The ratios have been corrected for K and π decay between the target and the final scintillator and for muon contamination.

Production angle	Target	Momentum (Bev/c)	Production ratio, at target K^+/π^+	K^-/π^-	$\bar{p}/\pi^-$
13°	Al	3.0	0.27 ±0.02		
		4.5			0.013 ±0.002
		6.0	0.29 ±0.05	0.062 ±0.010	0.014 ±0.002
		9.0	0.31 ±0.04	0.048 ±0.010	0.013 ±0.007
20°	Be	1.25	0.027 ±0.012	0.012 ±0.005	
		2.5	0.230 ±0.012	0.088 ±0.009	0.0051 ±0.0015
		3.0		0.088 ±0.010	

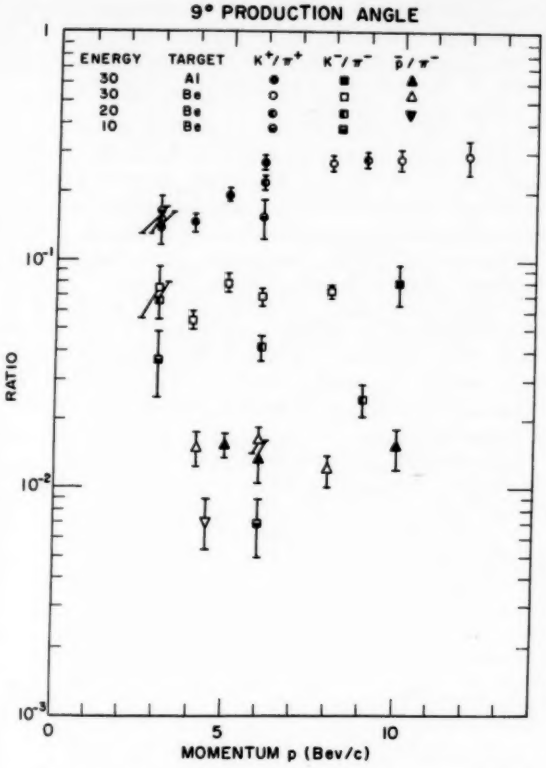

FIG. 3. The production ratios at the target of K^+/π^+, K^-/π^-, and $\bar{p}/\pi^-$ at various momenta, at 9° production angle. The ratios have been corrected for K and π decay between the target and the final scintillator and for muon contamination.

tillator so that the values plotted represent the production ratios at the target.

It can be seen from Fig. 1 that, where comparisons can be made, the characteristics of the pion spectra from the beryllium target and from the aluminum target are almost the same, except that

$$\left(\frac{d^2N}{dpd\Omega}\right)_{\text{Be}} \Big/ \left(\frac{d^2N}{dpd\Omega}\right)_{\text{Al}} \approx 1.1 - 1.4.$$

Part of these apparent differences between Al and Be targets may be due to relative monitoring and beam normalization errors and to fluctuations in target efficiency. The ratios K^+/π^+, K^-/π^-, and $\bar{p}/\pi^-$ can be seen from Figs. 2 and 3 to be insensitive to the difference between an aluminum and a beryllium target. In view of this insensitivity of particle production to target material and from general considerations based on the optical model, it appears that an analysis of the data in terms of a collision of the incident proton with a single nucleon of the target nucleus may be of interest and may reveal some significant characteristics of high-energy proton-nucleon interactions.

If one transforms the pion spectra to the proton-nucleon c.m. system, one finds that the pion spectra exhibit a low-energy peak $\lesssim 500$ Mev/c in the c.m. system, although the available kinetic energy ≈ 6 Bev. Furthermore the angular distribution is peaked in the forward direction. The c.m. angular and momentum distributions of the pions appear to be consistent with a limited mean transverse momentum transfer $\lesssim 0.5$-1 Bev/c.

From Figs. 2 and 3 it is clear that the K^+/π^+ ratios are not strongly sensitive to incident proton energy and tend to increase toward higher K^+ momenta. For 20-30 Bev incident proton energy, typical measured values of the K^+/π^+ ratio vary from 0.05 to 0.3. On the other hand, the K^-/π^- ratio falls rapidly with decreasing incident proton energy and also falls rapidly with increasing K^- momentum. Typical measured values of the K^-/π^- ratio vary from 0.08 to 0.02. At a given production angle the K^-/π^- and K^+/π^+ ratios tend to approach equality at very low momenta. These results may imply that the production of low-momentum K mesons occurs predominantly through K-pair production, while in the production of high-momentum K^+ mesons associated production (K-hyperon production) predominates.

For $\bar{p}/\pi^-$ ratios typical values are ~0.01-0.015 at low $\bar{p}$ momenta, falling to ~0.001 at high momenta. The $\bar{p}/\pi^-$ ratios are sensitive to the incident proton energy, dropping rapidly at the higher $\bar{p}$ momenta when the incident proton energy is reduced from 30 Bev to 20 Bev. This result is understandable when one recalls that the $\bar{p}$-p threshold in the c.m. system is 1.88 Bev.

Comparisons can be made between the results presented here and the results of some investigations[1] performed at CERN at 25-Bev proton energy using an Al target. At 6° lab production angle, three CERN K^-/π^- ratios were reported —at 5, 6, and 8 Bev/c. These data seem to lie reasonably between our data at 30-Bev and 20-Bev incident proton energy. Of the four CERN K^+/π^+ ratios reported by von Dardel et al.,[1] the ratio at 5 Bev/c is higher than our result by a factor ≈ 1.5. However, the CERN K^+/π^+ ratios at 6 and 8 Bev/c agree reasonably well with our results.

The CERN $\bar{p}/\pi^-$ ratios at 6° lab production angle, at 6, 8, and 11 Bev/c, are in agreement with our data, but the CERN point at 16 Bev/c appears to be higher than the trend of our data. The $\bar{p}/\pi^-$

ratios measured at CERN at 16° lab production angle by Cocconi et al.[1] are reasonably consistent with the trend of our measurements at production angles of 13° and 20°.

A more complete account of this work will be published elsewhere.

We wish to acknowledge the invaluable cooperation of the AGS staff and operating crew which made this investigation possible.

---

*On leave from Max-Planck Institut für Physik, Munich, Germany.

†This work was performed under the auspices of the U. S. Atomic Energy Commission.

[1]Similar investigations have been carried out at CERN: L. Gilly, B. Leontic, A. Lundby, R. Meunier, J. P. Stroot, and M. Szeptycka, Proceedings of the 1960 Annual International Conference on High-Energy Physics at Rochester (Interscience Publishers, Inc., New York, 1960), p. 808; G. von Dardel, R. M. Mermod, G. Weber, and K. Winter, Proceedings of the 1960 Annual International Conference on High-Energy Physics at Rochester (Interscience Publishers, Inc., New York, 1960), p. 837; V. T. Cocconi, T. Fazzini, G. Fidecaro, M. Legros, N. H. Lipman, and A. W. Merrison, Phys. Rev. Letters 5, 19 (1960).

[2]The $4\frac{3}{4}°$ and 20° experiments were performed by S. J. Lindenbaum, W. A. Love, J. A. Niederer, S. Ozaki, J. J. Russell, and L. C. L. Yuan. The 9° and 13° experiments were performed by W. F. Baker, R. L. Cool, E. W. Jenkins, T. F. Kycia, D. Lüers, and A. L. Read.

[3]The Čerenkov counters are described in D. A. Hill, D. O. Caldwell, D. H. Frisch, L. S. Osborne, D. M. Ritson, and R. A. Schluter, Rev. Sci. Instr. 32, 111 (1961); T. F. Kycia and E. W. Jenkins, paper presented at the International Conference on Nuclear Electronics at Belgrade, Yugoslavia, May, 1961 (unpublished), and Brookhaven National Laboratory Report BNL-5493 (unpublished); S. J. Lindenbaum and L. C. L. Yuan, in Methods of Experimental Physics (Academic Press, Inc., New York, to be published), Vol. 5A, Sec. 1.5.1; and S. J. Lindenbaum, W. A. Love, J. A. Niederer, S. Ozaki, J. J. Russell, and L. C. L. Yuan (to be published).

[4]H. J. Halama, Brookhaven National Laboratory Accelerator Development Department Internal Report HJH-1 (unpublished), and private communication.

[5]J. B. Cumming, G. Friedlander, J. Hudis, and A. Poskanzer (private communication).

[6]E. D. Courant (private communication).

[7]These remarks are based on the results of the IBM-704 program BEAM written by E. D. Courant [Brookhaven National Laboratory Accelerator Development Department Internal Report EDC-36 (unpublished), and private communication].

FAST ATOMIC TRANSITIONS WITHIN μ-MESONIC HYPERFINE DOUBLETS, AND OBSERVABLE EFFECTS OF THE SPIN DEPENDENCE OF MUON ABSORPTION*

R. Winston and V. L. Telegdi
The Enrico Fermi Institute for Nuclear Studies, The University of Chicago, Chicago, Illinois
(Received June 19, 1961)

It has been pointed out by Bernstein, Lee, Yang, and Primakoff,[1] that the two members $F_{\pm}=I\pm\frac{1}{2}$ of the hyperfine doublet ground state of a μ-mesonic atom with nonzero nuclear spin I could exhibit different disappearance rates $\Lambda_{\pm}$ as a consequence of the possible spin dependence of the interaction responsible for muon absorption. In particular, the now currently favored "universal" V-A interaction would lead to $\Lambda_{+}<\Lambda_{-}$. Bernstein et al.[1] made the implicit assumption that atomic processes inducing transitions between the two states $F_{\pm}$ were negligibly slow. With this assumption, they predicted that a logarithmic plot of the time dependence of the electron rates from negative muons stopped in a monoisotopic target of nonzero I should exhibit a positive curvature, corresponding to the superposition of the two exponentials characterized by Λ_{+} and Λ_{-}. Experimental detection of such a curvature could serve as a proof of the spin dependence of the absorption interactions but would give no clue to its more detailed nature.

It was subsequently pointed out[2] that, at least for the targets of experimental interest, the assumption of a negligibly slow transition rate between the two states $F_{\pm}$ is not a valid one. It was shown that the magnetic interaction between the "core" (=nucleus+muon) of the mesonic atom and its outer s electrons provides a sizeable conversion rate R between those two states. An explicit calculation for the case of $_{13}Al^{27}$ was presented in reference 2, made under the assumption that only the 3s (conduction) electrons of this target would effectively contribute to R. The magnitude of R so calculated was comparable to that of the difference $|\Lambda_{-}-\Lambda_{+}|\equiv|\Delta\Lambda|$. As was emphasized in reference 2, this parent-daughter relationship would lead to a negative curvature in the

experiment proposed by Bernstein et al. if the state F_- disappeared faster, which is precisely the prediction of the V-A interaction for a nucleus with positive magnetic moment μ_I.

Thus, the curvature experiment could possibly provide the as yet missing evidence that the V-A interaction governs muon capture. Some preliminary experimental evidence from Chicago, indicating the actual observation of negative curvature in Al and P, was discussed at the 1960 Rochester Conference.[3] Subsequent more refined measurements[4] performed in this laboratory indicate, however, that this preliminary "evidence" was due to spurious instrumental effects, the nature of which is now understood. This situation leads to the following questions: (a) Granting that muon capture is governed by the V-A interaction, what modification of the plausible rate calculation in reference 2 can account for the nonobservation of negative curvature? (b) Granting that a modified (and presumably reliable) rate calculation can account for this, what modification of the experiment originally proposed by reference 1 would lead to an observable negative curvature, thus confirming V-A? The present note purports to answer these questions.

(a) Conversion rate calculation. The problem of the transition rate between the states $F_\pm$ of interest, separated by an energy ϵ, is entirely analogous to that of an $M1$ transition between two nuclear states, the "core" playing here the role of the nucleus. However, the radiative transition rate R' is here readily calculable[5]:

$$R' = \tfrac{4}{3}\alpha^5 m_\mu^{-2} I/(2I+1)\epsilon^3, \tag{1}$$

while the conversion coefficients (that would yield R) are not available for the very soft ($\epsilon \lesssim 1$ kev) photons in question from standard tables.[6] We must, as was done in reference 2, estimate the rate $R_{i\to f}$ at which the magnetic hyperfine interaction between the "core" and an electron of the mesonic atom leads to electron ejection:

$$R_{ns\to ks} = \tfrac{1}{3}\pi\alpha^{-1}R'\epsilon^{-3}|u_{ns}(0)|^2|u_{ks}(0)|^2\rho_E(k), \tag{2a}$$

$$R_{np_{1/2}\to kp} = \tfrac{1}{3}\pi\alpha^{-1}R'\epsilon^{-3}(33/2)\left|\int_0^\infty u_{np}r^{-3}u_{kp}r^2dr\right|^2\rho_E(k), \tag{2b}$$

$$R_{np_{3/2}\to kp} = \tfrac{1}{3}\pi\alpha^{-1}R'\epsilon^{-3}(69/10)\left|\int_0^\infty u_{np}r^{-3}u_{kp}r^2dr\right|^2\rho_E(k). \tag{2c}$$

The approximation in the above expressions consists in taking the proper nonrelativistic limits, neglecting retardation effects and dropping contributions from nuclear magnetic moments. The rates in (2) are already summed over the electrons of the pertinent atomic shells, assumed to be filled; the total conversion rate is clearly

$$R = \sum R_{nlj\to klj'}, \tag{3}$$

where the sum is taken over all ionizable shells (nlj); ionizable means that the "edge" E_{nlj} lies below the available energy

$$\epsilon = E(F_+) - E(F_-) \simeq \tfrac{2}{3}\alpha^2 m_p^{-1} m_\mu^{\ 2}(\mu_I/\mu_B)(2I+1)/IZ_{\text{eff}}^{\ 3}, \tag{4}$$

where $Z_{\text{eff}}^{\ 3} = Z_{\text{eff}}^{\ 4}/Z$ taken from μ capture.[7] The replacement of Z^3 by $Z_{\text{eff}}^{\ 3}$ corrects for the finite nuclear size. For a completely general discussion, see Bohr and Weisskopf.[8]

We estimate R_n, the conversion rate for a given shell n, by the following approximate expressions valid for $|\epsilon - V_0| \ll Z'^2/2$:

$$|u_{ns}(0)|^2 \simeq 4Z'(Z'-S)^2/n^3, \quad |u_{ks}(0)|^2\rho_E(k) \simeq 4Z', \tag{5a}$$

where $Z' \equiv Z - 1$, the charge of the mesonic atom core, and

$$\left|\int_0^\infty u_{np}r^{-3}u_{kp}r^2dr\right|^2\rho_E(k) \simeq Z'^2(Z'-S)^2/9n^3, \tag{5b}$$

so that

$$R_{np\to kp} \simeq 0.16 R_{ns\to ks}. \tag{5c}$$

Here, S = inner, V_0 = outer Slater screening constants. These estimates are straightforward generalizations to off-diagonal matrix elements of Goudsmit's semiclassical hyperfine formula, justified by Fermi and Segrè via the JWKB method.[9] For the shielding of the emitted s electron, the remarks of Rose[10] are pertinent. In reference 2, R was calculated from (2a), assuming that only the $3s$ electrons of Al (magnetic M_{I} shell conversion) could be ejected. Inasmuch as $\epsilon(\text{Al}) \simeq 260$ ev while $E_{2S_{1/2}} = 88.60$ ev (exp. L_{I}-edge of Mg[11]), this assumption was in error. Using (3), (4), and (5), one finds:

$$R_2 \simeq 3.2\times 10^7 \text{ sec}^{-1} \text{ for } {}_{13}\text{Al}^{27} \tag{6}$$
$$(Z' = 12,\ S = 4.15,\ V_0 = 120 \text{ ev}).$$

The numerical value (6) far exceeds that calcula-

ted in reference 2, viz., $R = 6.2\times10^5$ sec^{-1}. It is two orders of magnitude larger[12] than $|\Delta\Lambda|$ and this fact, as we shall show later, accounts for the absence of observed negative curvature in Al. For $_{15}P^{31}$ the situation is entirely similar.

$R \gg |\Delta\Lambda|$ is not restricted to Al and P but holds quite generally for odd-Z nuclei of interest throughout the periodic table. This is due to the fact that whenever s conversion can occur, it does so at a rate that greatly exceeds $|\Delta\Lambda|$ (specifically disregarding nuclei with anomalously small μ_I). Since R_n increases with Z more rapidly than does $|\Delta\Lambda| \sim Z_{\text{eff}}^3$, it is sufficient to show this for the lowest Z at which a particular n, s shell can first be ionized. Thus, for $Z<9$, conversion occurs first at $Z \doteq 5$; for $_5B^{11}$, $R_2 \simeq 1.7\times10^5$ sec^{-1}, $\Delta\Lambda \simeq 5\times10^3$ sec^{-1}. For $9 \leq Z \leq 15$, $2s$ conversion always occurs; for $_9F^{19}$, $R_{2S} \simeq 2.9\times10^6$ sec^{-1}, $\Delta\Lambda \simeq 1.1\times10^5$ sec^{-1}. For $17 \leq Z < 39$, $3s$ conversion always occurs; for $_{17}Cl^{35}$, $R_{3S} \simeq 7.5\times10^6$ sec^{-1}, $\Delta\Lambda \simeq 2.3\times10^5$ sec^{-1}. For $39 \leq Z \leq 75$, $4s$ conversion always occurs; for $_{39}Y^{89}$, $R_4 \simeq 4.1\times10^7$ sec^{-1}, $\Delta\Lambda \simeq 2.8\times10^5$ sec^{-1}. Since the observable effects will be shown to decrease as $1/Z$, we do not consider very high values of Z.

The high conversion rates ($R \gg |\Delta\Lambda|$) discussed exclude practically observable effects in the time distribution of decay events, quite independently of the nature of the μ-capture interaction. Assuming $\mu_I > 0$, the time dependence of the populations in the $F_\pm$ states is governed by the equations

$$n_+(t) = n_+(0)e^{-(\Lambda_+ + R)t},$$

$$n_-(t) = [n_-(0) + n_+(0)R(R-\Delta\Lambda)^{-1}]e^{-\Lambda_- t} - n_+(0)R(R-\Delta\Lambda)^{-1}e^{-(\Lambda_+ + R)t}, \quad (7)$$

where $n_\pm(0)$ are the statistical weights of the states $F_\pm$. In the limit that $R \gg |\Delta\Lambda|$, the time distribution of the decay events (i.e., the electron rate) to order $\Delta\Lambda/R$ is

$$N^{\text{dec}}(t) \sim e^{-\Lambda_- t}(1 - Ae^{-Rt}), \quad (8)$$

where $A \equiv n_+(0)\Delta\Lambda/R$. The smallness of the amplitude A together with its rapid decay (in $_{13}Al^{27}$, $A \simeq 2\times10^{-3}$, $R^{-1} \simeq 3\times10^{-8}$ sec) accounts for the absence of observed negative curvature in $_{13}Al^{27}$ and $_{15}P^{31}$. As emphasized above, this smallness is not restricted to these nuclides.

(b) Experiments leading to observable negative curvature. Contrary to the study of the time distribution of the decay events, as originally proposed in reference 1, a study of the time distribution of capture events (capture neutrons and gamma rays) can lead to practically observable spin-dependence effects and, in particular, exhibit negative curvature. One has for these events from (7), again in the limit $R \gg \Delta\Lambda$,

$$N^{\text{cap}}(t) \sim e^{-\Lambda_- t}(1 - A'e^{-Rt}), \quad (9)$$

where $A' \equiv [n_+(0)\Delta\Lambda/\bar{\Lambda}^{\text{cap}}]/[1 + n_+(0)\Delta\Lambda/\bar{\Lambda}^{\text{cap}}]$; $\bar{\Lambda}^{\text{cap}} \equiv n_+(0)\Lambda_+^{\text{cap}} + n_-(0)\Lambda_-^{\text{cap}} \equiv$ mean capture rate. The striking difference between (8) and (9) is that A' may be a large amplitude of order unity. It is easy to see how this comes about:

When $|\Delta\Lambda|/R \ll 1$, the muon population is for $t \gg R^{-1}$ captured almost entirely from the F_- state at a rate $\Lambda_-^{\text{cap}}e^{-\Lambda_- t}$. Extrapolating back to $t=0$, this would require an initial capture rate Λ_-^{cap}, whereas the true initial capture rate is $\bar{\Lambda}^{\text{cap}}$. Therefore, $1 - A' = \bar{\Lambda}^{\text{cap}}/\Lambda_-^{\text{cap}}$, where $A' = [n_+(0)\Delta\Lambda/\bar{\Lambda}^{\text{cap}}]/[1 + n_+(0)\Delta\Lambda/\bar{\Lambda}^{\text{cap}}]$ as in (9). The same argument applied to decay events shows that $A \approx 0$ to zeroth order in $\Delta\Lambda/R$, since the decay probability is the same in both F states. Since A' decreases as $1/Z$, the effect is best studied in low-Z elements. For statistical efficiency, R should not greatly exceed Λ_-. Several elements (e.g., $_9F^{19}$) appear to be suited in practice for such experiments.

We conclude with two remarks:

(i) If one had $\Lambda_+/R \gg 1$, targets with $I = \frac{1}{2}$ (e.g., $_9F^{19}$ and $_{15}P^{31}$) should exhibit[13] a μ-decay asymmetry parameter $\alpha(I)$ half as large as $\alpha(0)$, the corresponding parameter for $I=0$. With $\Lambda_+/R \approx 1$, one should see a "damping" of the precession in the F_+ state, while $\Lambda_+/R \ll 1$ would imply $\alpha(\frac{1}{2}) \simeq 0$. In the case of $_{15}P^{31}$ ($\Lambda_+/R \simeq 0.03$), both $\alpha(\frac{1}{2})/\alpha(0) \approx 0.5$[14] and $\alpha(\frac{1}{2})/\alpha(0) \approx 0$[15] have been reported, while recent Liverpool results on $_9F^{19}$ ($\Lambda_+/R \approx 0.25$) are consistent with $\alpha(\frac{1}{2})/\alpha(0) \approx 0$.[16]

(ii) With $\Lambda_+/R \ll 1$, virtually all muons should be absorbed from the F_- state (assuming $\mu_I > 0$). The V-A interaction predicts $\Lambda_- > \Lambda_+$; thus on a plot of the reduced capture rates $\Lambda^{\text{cap}}/Z_{\text{eff}}^4$ vs neutron excess $(A-Z)/2A$, such nuclei as $_9F^{19}$, $_{11}Na^{23}$, $_{13}Al^{27}$, and $_{15}P^{31}$ should lie above the "Primakoff line."[17] Some evidence for this has been obtained recently,[4] but a quantitative comparison with theory does not appear possible at the present time.

We wish to thank Professor H. Primakoff and Professor G. Wentzel as well as J. L. Lathrop and R. A. Lundy for helpful comments and discussions.

*Research was supported by a joint program of the Office of Naval Research and the U. S. Atomic Energy Commission.

[1]J. Bernstein, T. D. Lee, C. N. Yang, and H. Primakoff, Phys. Rev. 111, 313 (1958).

[2]V. L. Telegdi, Phys. Rev. Letters 3, 59 (1959).

[3]V. L. Telegdi, Proceedings of the 1960 Annual International Conference on High-Energy Physics at Rochester (Interscience Publishers, Inc., New York, 1960), p. 713.

[4]J. L. Lathrop, R. A. Lundy, V. L. Telegdi, R. Winston, and D. D. Yovanovitch, this issue [Phys. Rev. Letters 7,107 (1961)].

[5]We use atomic units throughout: $m=m_e$, $l=\hbar^2/me^2$, $t=\hbar^3/me^4$.

[6]M. E. Rose, Internal Conversion Coefficients (Interscience Publishers, Inc., New York, 1958).

[7]J. C. Sens, Phys. Rev. 113, 679 (1958).

[8]A. Bohr and V. F. Weisskopf, Phys. Rev. 77, 94 (1950).

[9]Our estimates are in good agreement with available Hartree-Fock calculations of the relevant atomic wave functions; e.g., for $Z=12$ these give $|u_{2s}(0)|^2=400$ [W. Jacque Yost, Phys. Rev. 58, 557 (1940)], while our estimate is $|u_{2s}(0)|^2\simeq 370$.

[10]M. E. Rose, Phys. Rev. 49, 727 (1936).

[11]D. H. Tomboulian, Handbuch der Physik, edited by S. Flügge (Springer-Verlag, Berlin, 1957), Vol. 30, p. 246.

[12]We use the estimate of reference 1 throughout: $\Delta\Lambda/\Lambda^{cap}\simeq(2I+1)/IZ$ for $I=L+\frac{1}{2}$, $(2I+1)/(I+1)Z$ for $I=L-\frac{1}{2}$, assuming V-A.

[13]V. L. Telegdi, Proceedings of the International Conference on Mesons and Recently Discovered Particles, Padua-Venice, September 22-28, 1957 (Società Italiana di Fisica, Padua-Venice, 1958). H. Überall, Phys. Rev. 114, 1640 (1959). For $I>\frac{1}{2}$, similar remarks apply, but the asymmetry in either F state becomes very small. It must be remembered that the "damping" of precession may be due to either conversion or relaxation phenomena.

[14]L. V. Egorov, A. E. Ignatenko, and D. Chultém, J. Exptl. Theoret. Phys. (U.S.S.R.) 37, 1517 (1959) [translation: Soviet Phys.-JETP 37(10), 1077 (1960)].

[15]J. L. Lathrop, R. A. Lundy, V. L. Telegdi, and R. Winston, J. Exptl. Theoret. Phys. (U.S.S.R.) (to be published).

[16]A. Astbury, I. M. Blair, M. Hussain, M. A. R. Kemp, and H. Muirhead (to be published).

[17]H. Primakoff, Revs. Modern Phys. 31, 802 (1959).

MEASUREMENTS OF MUON DISAPPEARANCE RATES vs TIME IN C, Mg, Al, Si, AND P†

J. L. Lathrop, R. A. Lundy, V. L. Telegdi, R. Winston, and D. D. Yovanovitch

The Enrico Fermi Institute for Nuclear Studies, The University of Chicago, Chicago, Illinois

(Received July 13, 1961)

At the 1960 Rochester Conference we reported[1] some preliminary evidence for the observation of a hyperfine structure (i.e., spin dependence) effect in the capture of muons by $_{13}Al^{27}$ and $_{15}P^{31}$. This effect[2] consists in a (negative) curvature[3] K of the plot of $f(t)$, the logarithm of the electron rate from these targets, vs time,

$$K=K(0)=f''(1+f'^2)^{-3/2} \text{ at } t=0, \qquad (1)$$

and depends on the physical rates as follows:

$$K=K(\Delta\Lambda,R)=-2^{-3/2}n_+(\Delta\Lambda/\bar{\Lambda})(R-n_-\Delta\Lambda)/\bar{\Lambda}, \qquad (2)$$

where $n_\pm$ are the statistical weights of the hyperfine states $F_\pm=I\pm\frac{1}{2}$, $\bar{\Lambda}=n_+\Lambda_++n_-\Lambda_-$ the mean disappearance rate, $\Delta\Lambda=\Lambda_--\Lambda_+$, and R is the conversion rate from F_+ to F_- (assuming a positive nuclear magnetic moment).[4]

We have now repeated these "curvature" measurements under greatly improved conditions, and have found that, to within experimental error, $K=0$ for Al and Mg. We used the experimental setup schematically indicated in Fig. 1. The most essential improvements were the following ones:

(a) Comparison of the Al target ($I=\frac{5}{2}$) data with Mg data (mostly $I=0$) obtained under essentially identical conditions. In the past, C reference

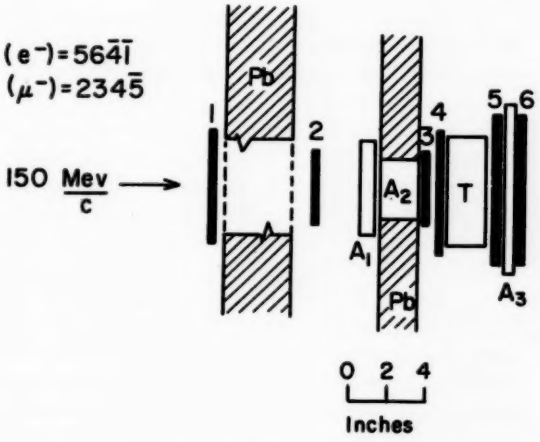

FIG. 1. Experimental setup. 1, 2, 3, 4, 5, and 6, square scintillation counters; $A_1=\frac{3}{4}$-in. Cu moderator, $A_2=2$-in. graphite moderator, $A_3=\frac{1}{2}$-in. polythene absorber. Pb = Pb collimators. $(\bar{1}\bar{4}56)$ = electron coincidence, $(234\bar{5})$ = muon coincidence.

Table I. Experimental results on curvature in Mg and Al.

Target	$K \times 10^3$	Accidental background (% at $t=0$)	Carbon background (% at $t=0$)
Mg	$+(1.1 \pm 1.0)$	0.209 ± 0.002	0.09 ± 0.38
Al	$+(2.4 \pm 1.7)$[a]	0.295 ± 0.004	0.03 ± 0.29

[a]To be compared with the value $K = -(4.4 \pm 1.0) \times 10^{-3}$ given in reference 1.

targets had been used to get "uncurved" data; however, C targets can show no background from muon decays in carbon—an essentially inevitable phenomenon with all other targets. This carbon background could simulate negative curvature through reduced reliability in fitting the time distribution.

(b) Improved time range of observation. To get a better evaluation of the flat, accidental background, an interval of 9 μsec was observed at $t<0$ (i.e., before the arrival of each muon). A longer (16-μsec) time range at $t>0$ was made available for observation in order to make the data statistically more valuable for separation (by least-squares program) into flat accidental background and exponential carbon background. Accidental backgrounds from $t<0$ data and from fit to $t>0$ data were required to match.

(c) Improvements in "digitron,"[5,6] the clock used to measure the distribution of μ-e time intervals. These improvements, to be described in detail elsewhere,[6] consisted primarily in replacing the pulsed oscillator with a continuous oscillator and scaler controlled gate combination, and in general using dc coupled transistorized circuits.

(d) Reduction of accidental background, achieved both by providing additional protective circuits in "digitron" and by using a high duty-cycle (~20%) muon beam.[6]

(e) Reduction and direct measurement of carbon background. Directly measured carbon background and carbon background from least-squares fits to $t>0$ data were required to agree. Reduction was acheived by covering scintillators 4 and 5 with thin (1-mil) Ag foils and not using Scotch tape in addition thereto, as well as by increasing their anticoincidence efficiencies. The short-lived muons stopping in these Ag foils essentially do not contribute electrons to the $t>0$ range used in data reduction. The direct carbon background measurements were made with an "equivalent" Cu target. The short (Cu) and the long (C) components separate easily. Two layers of Scotch tape (16 mg/cm^2), added on the upstream face of counter 5, could readily be detected in the presence of a 9 g/cm^2 Cu target. This purposely created carbon background could be used to gauge the carbon background present in the actual (Mg and Al) runs.

To make the "curvature" (Al) and the "control" (Mg) runs as closely comparable as possible, the Al target consisted of 5 equally spaced $\frac{1}{4}$-in. thick sheets filling the same volume (6 in. $\times$ 6 in. $\times$ 2 in.) as the Mg target. Table I summarizes our most reliable data obtained with these targets; to within experimental error, $K=0$ in both Al and Mg—in contrast to our preliminary evidence for Al. A recent calculation of the conversion rate[7] yields $R(\mathrm{Al}) = 3.2 \times 10^7$ sec^{-1}. With this large value of R, $K(t)$ becomes a rapidly varying (decreasing) function of time.[4] Under these circumstances the "curvature" $\overline{K}$ obtained by fitting the electron time distribution over several mean lives is no longer given by (2) but rather by $\overline{K} = -2^{-3/2} n_+ \times (\Delta\Lambda/R)(\overline{\Lambda}/R)$. With the above value of R and the estimate[2] $\Delta\Lambda/\overline{\Lambda} = 0.17$, one has $\overline{K} \simeq -5 \times 10^{-5}$. This is in agreement with the null result in Table I.

In the course of our search for spin-dependent effects in muon capture, we have obtained rather precise μ lifetimes for C, Mg, Al, Si, and P. These, as well as some quantities derived from them, are summarized in Table II.

Table II. Precise μ^- lifetimes for C, Mg, Al, Si, and P.

Target	Lifetime[a] (μsec)	Capture rate[b] $\Lambda^{\mathrm{cap}} \times 10^{-5}$ (sec^{-1})	$\Lambda^{\mathrm{cap}}/\langle\rho\rangle$[c]
C	2.041 ± 0.005	0.361 ± 0.01	17.8 ± 0.5
Mg	1.071 ± 0.002	4.80 ± 0.02	19.4 ± 0.1
Al	0.864 ± 0.002	6.62 ± 0.03	21.4 ± 0.1
Si	0.767 ± 0.002	8.50 ± 0.03	19.9 ± 0.1
P	0.635 ± 0.002	11.21 ± 0.05	21.0 ± 0.1

[a]Statistical error computed from least-squares fit to data.

[b]Computed using the free muon decay rate, $\Lambda_{\mathrm{dec}} = (4.539 \pm 0.005) \times 10^5$ sec^{-1}.

[c]$\langle\rho\rangle$ as defined and given by J. C. Sens, Phys. Rev. 113, 679 (1959).

†Research was supported by a joint program of the Office of Naval Research and the U. S. Atomic Energy Commission.

[1]V. L. Telegdi, Proceedings of the 1960 Annual International Conference on High-Energy Physics at Rochester (Interscience Publishers, Inc., New York, 1960), p. 713.

[2]J. Bernstein, T. D. Lee, C. N. Yang, and H. Primakoff, Phys. Rev. 111, 313 (1958).

[3]V. L. Telegdi, Phys. Rev. Letters 3, 59 (1959).

[4]The time dependence of the electron rates can, of course, be characterized over a span of several mean lives by K as defined in (1) if, and only if, K is a slowly varying function of time. This is the case when $R \lesssim \bar{\Lambda}$, an assumption that appeared plausible[3] when these measurements were performed.

[5]R. A. Swanson, Rev. Sci. Instr. 31, 149 (1960).

[6]R. A. Lundy (to be published).

[7]R. Winston and V. L. Telegdi, preceding Letter [Phys. Rev. Letters 7,104 (1961)].

SEARCH FOR HIGH-ENERGY COSMIC GAMMA RAYS*

Thomas L. Cline†

Department of Physics and Laboratory for Nuclear Science,
Massachusetts Institute of Technology, Cambridge, Massachusetts

(Received June 19, 1961)

This note describes an attempt to detect gamma rays of cosmic origin in the energy region appropriate to π^0 decay. Since π^0 mesons are produced in nucleon-antinucleon annihilation, the existence or nonexistence of a gamma-ray flux from certain portions of the sky bears upon questions such as possible collisions between galaxies and antigalaxies[1] and cosmological models which postulate matter and antimatter creation.[2] New upper limits are set on the creation rate and on the density of interstellar antinucleons.

The existence of high-energy gamma rays in the primary cosmic radiation was first investigated by Schein, Jesse, and Wollan using G-M tubes,[3] by Hulsizer and Rossi using ionization chambers,[4] and by Critchfield, Ney, and Oleksa using cloud chambers.[5] These experiments set an upper limit for the flux of the electron-photon component above about 1 Bev at about 1% of the primary cosmic-ray flux. G-M telescopes were used by Perlow and Kissinger,[6] and more recently by Danielson.[7] All of these experiments suffered the disadvantages of either a high proportion of locally-produced background or an energy sensitivity which did not extend significantly into the 70-Mev region, and none had a directional survey of the sky as its purpose.

A cross section of the balloon-borne detector that was used in the present experiment is shown in Fig. 1. Incoming gamma rays, collimated by

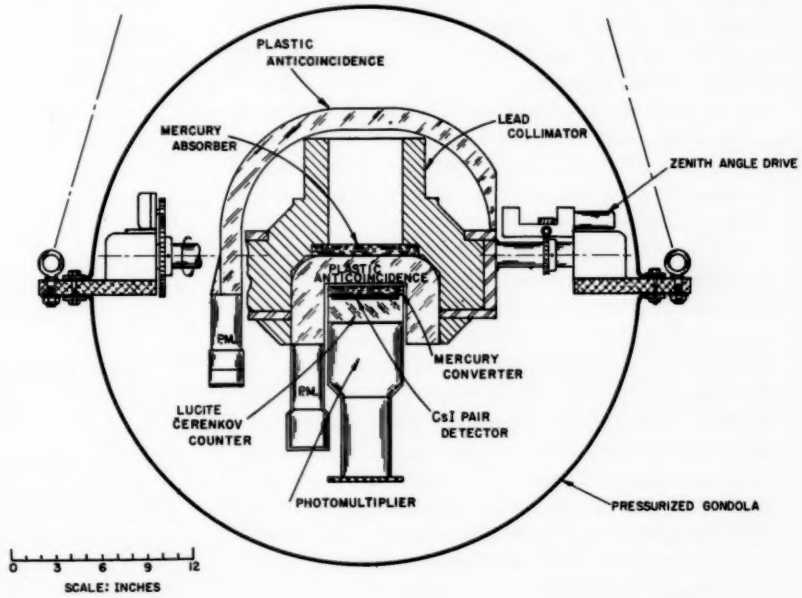

FIG. 1. Cross section of the apparatus. The geometrical figure for this telescope was 1.7 cm² sr.

the lead shield, produced electron pairs in either of two removable mercury radiators. The upper radiator, when inserted in flight, was used to measure the attenuation of the beam in order to identify the measured flux as photons. The lower radiator produced the pairs that were detected by the scintillator-Čerenkov combination at the bottom. A pulse corresponding to the traversal of two minimum-ionizing particles in the cesium iodide crystal was required in coincidence with a pulse from the Lucite Čerenkov counter. The pair detector was surrounded by an anticoincidence scintillator inside the lead shield. This anticoincidence requirement excluded incident charged particles as well as electron pairs or showers projected upwards from the detector. In addition, a large anticoincidence scintillator outside the lead shield was used to reduce the background produced by cosmic-ray interactions in that shield. The apparatus was rotated in flight to various zenith angles in order to pour the mercury in and out, to measure the zenith-angle dependence of the gamma-ray intensity and to measure the gamma-ray albedo.

The detection efficiency of the instrument was estimated as a function of gamma-ray energy from the known pair-production cross sections, electron multiple-scattering expressions, etc. This curve was combined with the experimentally determined energy spectrum of pair-producing gamma rays near the top of the atmosphere as measured in the emulsion experiments of Carlson, Hooper, and King,[8] and of Svensson.[9] The result was an effective efficiency of about 0.17. This efficiency differed by less than 10% with the substitution of the gamma-ray spectrum from low-energy proton-antiproton annihilation. The adequacy of the efficiency estimate was confirmed and the angular response of the instrument was measured in a π^0 decay gamma-ray beam at the MIT synchrotron.

The detector was balloon-borne at 55° geomagnetic latitude on July 1, 1960, for about one day of which 12 hours were spent at 8.5 g cm^{-2} atmospheric depth. Evidence that gamma rays were detected is as follows: The counting rate as a function of atmospheric depth, shown in Fig. 2, followed a transition curve having a maximum near 180 g cm^{-2}, entirely similar to that of the electron-photon component. The ratio of the counting rate with the upper mercury absorber inserted to the rate with this absorber removed was 0.40 ± 0.07, while the expected ratio for pure gamma-ray detection was 0.35. The gamma-ray albedo flux was measured and found to be in agreement with the results of the emulsion experiment of Svensson, having a value of about half that of the vertically downward gamma-ray flux at 14 g cm^{-2}.

The gamma-ray intensity versus atmospheric depth in the region 0 to 40 g cm^{-2} is shown in the inset of Fig. 2. The four measurements with the smallest indicated errors were taken at four zenith angles while the balloon floated at 8.5 g cm^{-2}. Since the corresponding atmospheric depths are small compared with any of the characteristic interaction lengths involved, a linear extrapolation to 0 g cm^{-2} is justified. The extrapolated intensity, determined by a least-squares fit, is $(1 \pm 3) \times 10^{-3}$ cm^{-2} sec^{-1} sr^{-1} and the corresponding upper limit to the gamma-ray intensity inci-

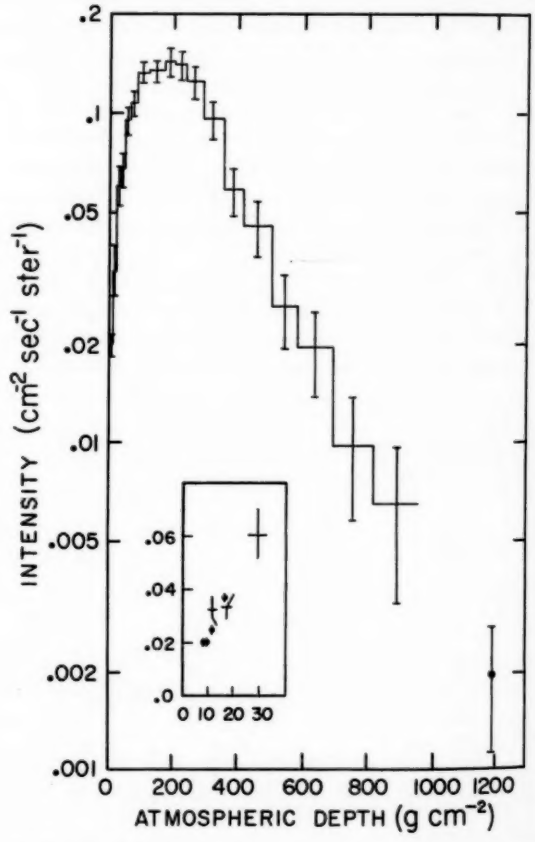

FIG. 2. Gamma-ray intensity versus atmospheric depth. (The axis of the detector was clamped at 30-degree zenith angle throughout the ascent, hence the 15% correction to depth.) The insert shows a linear plot of the intensity for small atmospheric depths; the units are the same for both graphs.

dent upon the top of the atmosphere, for a 95% statistical confidence limit, is 7×10^{-3} cm^{-2} sec^{-1} sr^{-1}. This value must be regarded as an average over the directions scanned, i.e., as a limit to the essentially isotropic intensity from the northern celestial hemisphere.

From a sidereal arrival direction analysis, the incident flux from the direction of Cygnus-A, having subtracted off the secondary flux, was found to be $(-2\pm7)\times10^{-4}$ cm^{-2} sec^{-1}, with the corresponding upper limit of 1.2×10^{-3} cm^{-2} sec^{-1} for a 95% statistical confidence limit. A previous upper limit, based upon the detection of one gamma ray, was set at 5×10^{-3} cm^{-2} sec^{-1} by Braccesi, Ceccarelli, and Salandin,[10] using emulsions. This corresponds to an upper limit of 1.5×10^{-2} cm^{-2} sec^{-1} for a 95% statistical confidence limit. Estimates of the flux from Cygnus-A, based on a galaxy-antigalaxy collision model, range from Morrison's value of about 1 cm^{-2} sec^{-1} to Savedoff's value,[11] which is yet three orders of magnitude below the upper limit set by this experiment.

Proton-antiproton annihilation taking place anywhere in the cone defined by the aperture of the instrument could also contribute to a gamma-ray intensity. The lifetime of an antiproton against annihilation with interstellar protons can be taken as $\tau=[nv(\sigma_0 c/v)]^{-1}$, where n is the proton number density, v is the relative velocity, and $\sigma=\sigma_0(c/v)$ is the annihilation cross section, in which σ_0 is about 10^{-25} cm^2. This lifetime is much greater than the time scale of the universe (1.4×10^{10} years) for proton densities appropriate to intergalactic space ($n\ll10^{-4}$ cm^{-3}), and is much less than the time scale of the universe for proton densities appropriate to the galaxy ($n\gg10^{-2}$ cm^{-3}). Within wide limits of proton densities, the annihilation frequency would therefore be constant within the galactic volume, so that the resulting annihilation gamma-ray flux depends only upon the geometrical shape of the galactic portion subtended by the aperture of the detector. The annihilation frequency, S, and the gamma-ray intensity, J, are related by $S=4\pi J(mRf)^{-1}$, where $m\geq3$ is the average number of gamma rays per annihilation, R is the distance to the surface of the galactic disk in the direction scanned, and f is a geometrical factor which takes into account the shape of the galaxy within the cone scanned. For the direction perpendicular to the galactic plane, $R=5\times10^{20}$ cm and $f=1$; for the direction of the galactic anticenter, $R=2\times10^{22}$ cm and $f=0.15$.

During the time that the balloon was near maximum altitude the aperture of the instrument scanned the galactic anticenter at certain known times, but, due to a partial loss of azimuth information, it was not possible to separate all of the data from the direction perpendicular to the galactic plane. However, an upper limit for each intensity can be established: The greater intensity would come from the galactic anticenter, so that a conservatively set upper limit results if the value for the isotropic intensity is treated as a value for the direction perpendicular to the galactic plane. With $J\leq7\times10^{-3}$ cm^{-2} sec^{-1} sr^{-1}, this gives $S\leq6\times10^{-23}$ cm^{-3} sec^{-1} as the upper limit to the annihilation frequency for the portion of the galaxy in the direction of the North Galactic Pole. This limit is independent of knowledge of the shape of the galaxy other than the perpendicular distance to the surface. An upper limit to the gamma-ray intensity from the direction of the galactic anticenter, for a 95% statistical confidence limit, was calculated to be 1.8×10^{-2} cm^{-2} sec^{-1} sr^{-1}. This value of J gives $S\leq2.5\times10^{-23}$ cm^{-3} sec^{-1} as the upper limit to the annihilation frequency for the galactic anticenter.

The product of the annihilation frequency, S, and the antiproton lifetime, τ, is the corresponding upper limit to the antiproton number density, $\bar{n}$. The result, which is a function of the proton number density, can be expressed as $\bar{n}=S(\sigma_0 cn)^{-1}\leq(8\times10^{-9})/n$ cm^{-3}. This upper limit to the interstellar antiproton density is a factor of ten below previous limits that assume $n\approx1$ cm^{-3}.[2]

The upper limit for the annihilation frequency of antiprotons can also be taken to be an upper limit for the creation rate of antiprotons. As long as the antiproton lifetime within the galaxy is short compared with the age of the galaxy, which seems certain for any proton density in excess of 10^{-2} cm^{-3}, an equilibrium between annihilation and any postulated long time-scale production mechanism should be established. The proton production rate has been required by steady-state cosmology to be about 3×10^{-22} cm^{-3} sec^{-1},[2] which is a factor of ten above the upper limit of 2.5×10^{-23} cm^{-3} sec^{-1} for antiproton annihilation (or production) reported here. The value of this required production rate in steady-state theory, however, depends upon the experimental determination of, e.g., the average universal mass density, which at present is uncertain and may be as much as a factor of 10^3 below the value of 10^{-28} to 10^{-29} g cm^{-3} assumed earlier by cosmologists.[12]

It is my great pleasure to thank Professor William L. Kraushaar for suggesting and guiding this work. I would like to thank many people for their contributing efforts, in particular, W. B. Smith, E. Mangan, R. Mudge, and Dr. M. S. Webster.

*Supported in part by the U. S. Atomic Energy Commission and by the Office of Naval Research.

†Present address: National Aeronautics and Space Administration, Goddard Space Flight Center, Greenbelt, Maryland.

[1]P. Morrison, Nuovo cimento 7, 858 (1958).
[2]F. Hoyle and G. R. Burbidge, Nuovo cimento 4, 558 (1956).
[3]M. Schein, W. P. Jesse, and E. O. Wollan, Phys. Rev. 59, 615 (1941).
[4]R. I. Hulsizer and B. Rossi, Phys. Rev. 73, 1402 (1948).
[5]C. L. Critchfield, E. P. Ney, and S. Oleksa, Phys. Rev. 85, 461 (1952).
[6]G. J. Perlow and C. W. Kissinger, Phys. Rev. 81, 552 (1951).
[7]R. E. Danielson, J. Geophys. Research 65, 2055 (1960).
[8]A. G. Carlson, J. E. Hooper, and D. T. King, Phil. Mag. 41, 701 (1950).
[9]G. Svensson, Arkiv Fysik 13, 347 (1958).
[10]A. Braccesi, M. Ceccarelli, and G. Salandin, Nuovo cimento 17, 691 (1960).
[11]M. P. Savedoff, Nuovo cimento 13, 12 (1959).
[12]A. Sandage, Astrophys. J. 113, 355 (1961).

SELF-CONSISTENT CALCULATION OF THE MASS AND WIDTH OF THE $J=1$, $T=1$, $\pi\pi$ RESONANCE

Fredrik Zachariasen*
California Institute of Technology, Pasadena, California
(Received June 28, 1961)

The existence of a $J=1$, $T=1$ resonance in $\pi\pi$ scattering now seems to be very probable, though there are still rather large uncertainties in its position and width.[1] From a theoretical point of view, one may believe this resonance to be due to the existence of an unstable vector meson,[2] called ρ, or one may say the resonance is dynamical.[3] If the ρ meson has an infinite bare mass, there is essentially no difference in the results of these two points of view.[4,5] The principal distinction between the two philosophies comes from the fact that if the ρ meson is really a new particle, its mass and coupling constant must be thought of as new independent parameters which can be chosen to be anything, while if the ρ is a dynamical resonance, the mass and coupling constant are determined by other parameters already in the theory.

Within the "dynamical" philosophy, attempts have been made to calculate the mass and coupling constant of the ρ meson.[3,6] These have not been entirely successful; furthermore, the most complete and careful attempt to do this,[3] based on the Mandelstam representation, involves the solution of a very complicated set of coupled integral equations on a computing machine, and is therefore not very transparent. One qualitative feature which has been emphasized by Chew and Mandelstam,[3] however, is that the existence of the resonance seems to follow from the operation of a "bootstrap mechanism," in which the strong force between two pions in a P state, which is needed to produce the resonance, is provided by the exchange of a pair of resonating pions.

In this way, the basic underlying source of the pion-pion interaction (which could, for example, be the $\lambda\phi^4$ interaction or a force produced by the exchange of a strongly interacting S-wave pion pair) does not seem to play a large quantitative role in the final results, but merely provides the spark which sets the bootstrap off. One would, therefore, expect to be able to obtain the ρ meson's properties as the result of a self-consistent calculation with no parameters.

It is our purpose here to apply the bootstrap mechanism in a very simple-minded and trivial calculation, which yields quantitative values for the ρ mass and coupling constant. The approximation is the following: a ρ meson, of mass m_ρ and coupled to the pion with a coupling constant $\gamma_{\rho\pi\pi}$, is exchanged between two pions as shown in Fig. 1.

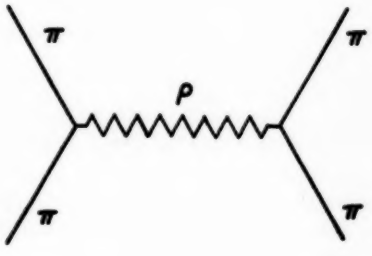

FIG. 1. The one ρ-meson exchange diagram.

The force thereby produced in the $J=1$, $T=1$ channel is attractive and depends on m_ρ and $\gamma_{\rho\pi\pi}$. If m_ρ and $\gamma_{\rho\pi\pi}$ are adjusted properly, this force may be made to produce a resonance at m_ρ with coupling constant $\gamma_{\rho\pi\pi}$. Thus we obtain two relations between m_ρ and $\gamma_{\rho\pi\pi}$ from which both may be determined.

In practice, the calculation is most easily carried out using the determinantal method.[7] One computes the determinantal function for the $J=1$, $T=1$ channel from the equation[8]

$$D\left(\frac{s}{m_\pi^2}, \gamma_{\rho\pi\pi}, \frac{m_\rho^2}{m_\pi^2}\right) = 1 + \frac{s-s_0}{\pi}\int_{4\mu^2}^{\infty} \frac{\mathrm{Im}D(s/m_\pi^2, \gamma_{\rho\pi\pi}, m_\rho^2/m_\pi^2)}{(s'-s_0)(s'-s-i\epsilon)}\,ds', \tag{1}$$

where s is the total c.m. energy squared,

$$\mathrm{Im}D = -(\sin\delta e^{i\delta})_1, \tag{2}$$

and $(\sin\delta e^{i\delta})_1$ is calculated from the graph of Fig. 1. Then we require

$$\mathrm{Re}D(m_\rho^2/m_\pi^2, \gamma_{\rho\pi\pi}, m_\rho^2/m_\pi^2) = 0, \tag{3}$$

and[8]

$$\frac{\mathrm{Im}D(m_\rho^2/m_\pi^2, \gamma_{\rho\pi\pi}, m_\rho^2/m_\pi^2)}{(d/ds)\mathrm{Re}D\big|_{s=m_\rho^2}} = \tfrac{1}{3}\left(\frac{\gamma_{\rho\pi\pi}^2}{4\pi}\right)\left(\frac{(m_\rho^2-4\mu^2)^3}{m_\rho^2}\right)^{1/2}. \tag{4}$$

Equations (3) and (4) together fix m_ρ and $\gamma_{\rho\pi\pi}$. The computation is explicit and straightforward, and an approximate numerical evaluation of the necessary two integrals yields

$$m_\rho \approx 950\ \mathrm{Mev}, \quad \gamma_{\rho\pi\pi}^2/4\pi \approx 2.8.$$

There are no parameters to be adjusted in obtaining these results, other than the pion mass which only provides a dimension. The numbers are in fair agreement with the present experimental data,[1] which indicate something like

$$m_\rho \approx 750\ \mathrm{Mev}, \quad \gamma_{\rho\pi\pi}^2/4\pi \approx 1.$$

The most serious deficiency of a calculation like this based on the determinantal method lies in the violation of crossing symmetry. One may hope, however, in analogy to other more or less successful calculations,[7] that this lack is not of great quantitative importance; in any case, it may be of value to illustrate by a simple method what it is that the complicated and more complete calculations are supposed to do if they can ever be successfully carried out.

In conclusion, it may be remarked that the "bootstrap" mechanism may be responsible for the existence of many, if not all, other particles as well; for example, the strange vector meson called M by Gell-Mann,[9] with isotopic spin $\frac{1}{2}$, may be a P-wave resonance in $K\pi$ scattering. There may, in addition, be an S-wave resonance or pseudoresonance, corresponding to a K' meson like the K but with opposite parity. In a complete calculation of the bootstrap in the $\pi\pi$ system, all of these particles, or resonances, should of course be included. For a more complete discussion of these points, see reference 5.

I should like to thank M. Gell-Mann for several comments and suggestions, and D. Sharp for the numerical calculations.

---

*Alfred P. Sloan Foundation Fellow.

[1]J. A. Anderson, V. X. Bang, P. G. Burke, D. D. Carmony, and N. Schmitz, Phys. Rev. Letters 6, 365 (1961); A. R. Erwin, R. March, W. D. Walker, and E. West, Phys. Rev. Letters 6, 628 (1961); G. F. Chew (private communication).

[2]J. J. Sakurai, Ann. Phys. 11, 1 (1960).

[3]G. F. Chew and S. Mandelstam, Phys. Rev. 119, 467 (1960), and University of California Radiation Laboratory Report UCRL-9126 (unpublished).

[4]M. Gell-Mann and F. Zachariasen, California Institute of Technology Synchrotron Laboratory Report CTSL-26, 1961 (unpublished).

[5]M. Gell-Mann (unpublished).

[6]M. Baker and F. Zachariasen, Phys. Rev. 118, 1659 (1960).

[7]M. Baker, Ann. Phys. 4, 271 (1958).

[8]The subtraction point s_0 is chosen at the end of the left-hand branch cut in ImD, in order that the coupling constant $\gamma_{\rho\pi\pi}$ is correctly related to the discontinuity due to the one ρ exchange contribution.

[9]M. Gell-Mann, California Institute of Technology Synchrotron Laboratory Report CTSL-20, 1961 (unpublished).